NASA
National
Aeronautics and
Space
Administration

CR-175002
SEPTEMBER 9, 1985
21-5477

THERMAL BARRIER COATING LIFE-PREDICTION MODEL DEVELOPMENT

FIRST ANNUAL REPORT

BY

T.E. STRANGMAN

AND

J. NEUMANN

FOR NASA LERC CONTRACT NAS3-23945

GARRETT

GARRETT TURBINE ENGINE COMPANY
A DIVISION OF THE GARRETT CORPORATION
PHOENIX ARIZONA

1189

1. Report No.	2. Government Accession No.	3. Recipient's Catalog No.
CR-175002		

4\. Title and Subtitle

Thermal Barrier Coating Life-Prediction Model Development Annual Report

5\. Report Date

September 9, 1985

6\. Performing Organization Code

7\. Author(s)

T.E. Strangman
J. Neumann

8\. Performing Organization Report No.

21-5477

9\. Performing Organization Name and Address

Garrett Turbine Engine Company
111 S. 34th Street, P.O. Box 5217
Phoenix, AZ 85010

10\. Work Unit No.

11\. Contract or Grant No.

NAS3-23945

12\. Sponsoring Agency Name and Address

NASA-Lewis Research Center

13\. Type of Report and Period Covered

Annual, First Year

14\. Sponsoring Agency Code

15\. Supplementary Notes

Project Manager: R.A. Miller
NASA-Lewis Research Center
Cleveland, Ohio 44135

16\. Abstract

This program focuses on predicting the lives of two types of strain-tolerant and oxidation-resistant TBC systems that are produced by commercial coating suppliers to the gas turbine industry. The plasma-sprayed TBC system, composed of a low-pressure plasma-spray (LPPS) applied oxidation resistant NiCrAlY bond coating and an air-plasma-sprayed yttria (8 percent) partially stabilized zirconia insulative layer, is applied by both Chromalloy (Orangeburg, New York) and Klock (Manchester, Connecticut). The second type of TBC is applied by the electron beam - physical vapor deposition (EB-PVD) process by Temescal (Berkeley, California).

The first year of this multiyear program was focused on literature review, specimen procurement, TBC system characterization, and nondestructive evaluation methods.

Thermomechanical and thermochemical testing of the program TBCs is now in progress. A number of the thermomechanical tests have been completed. Fracture mechanics data for the Chromalloy plasma-sprayed TBC system indicate that the cohesive toughness of the zironia layer is increased by thermal cycling and reduced by high temperature exposure at 1150C.

Eddy current technology feasibility has been established with respect to nondestructively measuring zirconia layer thickness of a TBC system.

High-pressure turbine blades have been coated with the program TBC systems for a "piggyback" test in a TFE731-5 turbofan factory engine test. Data from this test will be used to validate the TBC life models.

17. Key Words (Suggested by Author(s))	18. Distribution Statement
Thermal Barrier Life Prediction Development Program	

19. Security Classif. (of this report)	20. Security Classif. (of this page)	21. No. of Pages	22. Price*
UNCLASSIFIED	UNCLASSIFIED	61	

* For sale by the National Technical Information Service, Springfield, Virginia 22161

NASA-C-168 (Rev. 10-75)

TABLE OF CONTENTS

GARRETT TURBINE ENGINE COMPANY
A DIVISION OF THE GARRETT CORPORATION
PHOENIX, ARIZONA

LIST OF ILLUSTRATIONS

LIST OF ILLUSTRATIONS (Contd)

LIST OF ILLUSTRATIONS (Contd)

LIST OF TABLES

GARRETT TURBINE ENGINE COMPANY
A DIVISION OF THE GARRETT CORPORATION
PHOENIX, ARIZONA

THERMAL BARRIER COATING LIFE-PREDICTION MODEL DEVELOPMENT FIRST ANNUAL REPORT

1.0 SUMMARY

Thermal barrier coatings (TBCs) for turbine airfoils in high-performance engines represent an advanced materials technology with both performance and durability benefits. The foremost TBC benefit is the reduction of heat transferred into air-cooled components. To achieve these benefits, however, the TBC system must be reliable. Mechanistic thermomechanical and thermochemical life models and statistically significant design data are therefore required for the reliable exploitation of TBC benefits on gas turbine airfoils. Garrett's NASA-Host Program is designed to fulfill these requirements.

This program focuses on predicting the lives of two types of strain-tolerant and oxidation-resistant TBC systems that are produced by commercial coating suppliers to the gas turbine industry. The plasma-sprayed TBC system, composed of a low-pressure plasma-spray (LPPS) applied oxidation resistant NiCrAlY (or CoCrAlY) bond coating and an air-plasma-sprayed yttria (8 percent) partially stabilized zirconia insulative layer (Figure 1-1), is applied by both Chromalloy (Orangeburg, New York) and Klock (Manchester, Connecticut). The second type of TBC is applied by the electron beam - physical vapor deposition (EB-PVD) process by Temescal (Berkeley, California).

The first year of this multiyear program was focused on the following activities:

- Literature review
- Specimen procurement
- TBC system characterization
- Nondestructive evaluation methods

GARRETT TURBINE ENGINE COMPANY
A DIVISION OF THE GARRETT CORPORATION
PHOENIX, ARIZONA

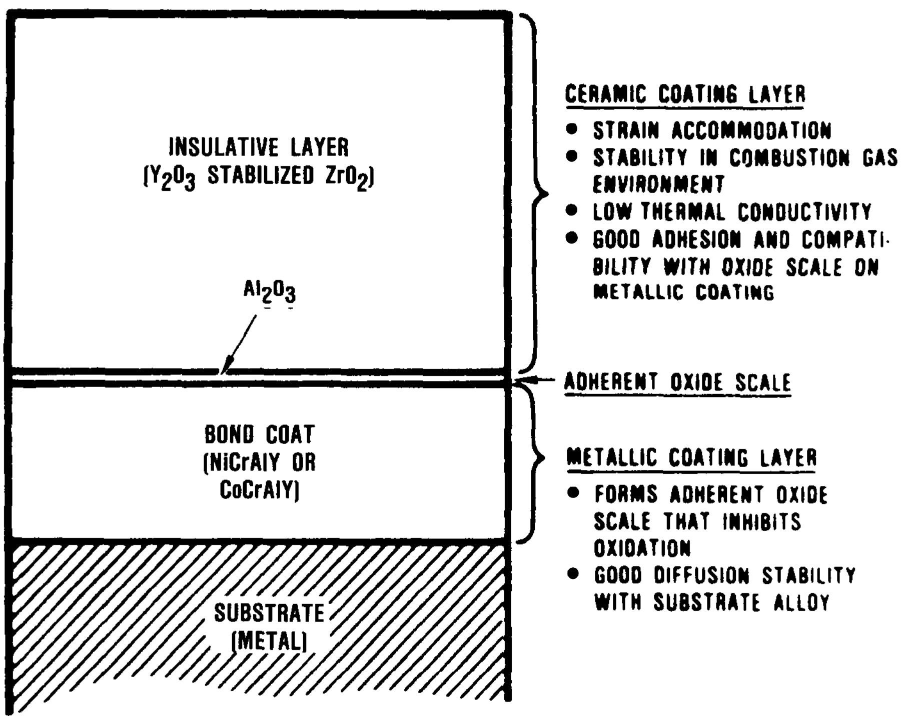

Figure 1-1. Constituents of a Thermal Barrier Coating System.

Thermomechanical and thermochemical testing of the program TBCs is now in progress. A number of the thermomechanical tests have been completed. Fracture mechanics data for the Chromalloy plasma-sprayed TBC system indicate that the cohesive toughness of the zirconia layer is increased by thermal cycling and reduced by high temperature exposure at 1150C.

Eddy current technology feasibility has been established with respect to nondestructively measuring zirconia layer thickness of a TBC system.

High-pressure turbine blades have been coated with the program TBC systems for a "piggyback" test in a TFE731-5 turbofan factory engine test. Data from this test will be used to validate the TBC life models.

2.0 INTRODUCTION

Thermal barrier coatings (TBCs) for turbine airfoils in high-performance engines represent an advanced materials technology that has both performance and durability benefits. Foremost of the TBC benefits is the reduction of heat transferred into air-cooled components. To achieve these benefits, however, the TBC system must be reliable. Mechanistic thermomechanical and thermochemical life models and statistically significant design data are therefore required for the reliable exploitation of TBC benefits on gas turbine airfoils. This 60-month program is designed to fulfill these requirements.

GTEC strategy for this program comprises the following objectives:

- Development of mission-analysis-capable thermochemical and thermomechanical TBC life models that recognize and account for all significant mission, engine, and component design factors. These parameters include temperature, time, six TBC strain components, turbine pressure, and aircraft altitude (salt ingestion).

- Development of rapid computation approaches for estimating TBC life during preliminary design iterations.

- Development of a comprehensive TBC life model to provide the desired accuracy for final component designs.

- Obtaining design data for plasma-sprayed and electron beam evaporation - physical vapor deposition (EB-PVD) TBC systems produced by commercial suppliers to the gas turbine industry; i.e., Chromalloy, Klock, and Temescal.

- o Development of affordable tests to obtain the statistically significant design data required to calibrate TBC life models.

The program consists of two phases. Phase I, Failure Mode Analyses and Model Development (Tasks I - V and A), is a 36-month technical effort and focuses on experimentally quantifying plasma-sprayed and EB-PVD failure modes and on developing engine-mission-analysis-capable preliminary TBC life prediction models for major failure modes. Task A is a GTEC-funded task providing for coating HP turbine blades with the specific coating systems selected for Phase I and conducting piggyback factory engine tests to provide data to verify the TBC life prediction model's accuracy.

Phase II, Design-Capable Life Models (Tasks VI-XI and B), is a 24-month optional effort to be exercised by NASA at the end of Phase I. It provides for additional experimental quantification of failure modes in plasma-sprayed TBCs and development of a comprehensive, mission-capable model with the desired accuracy for final designs. The mission-analysis capability of the TBC life model will be validated with analyses of multitemperature burner rig tests and factory test engine experience. In addition, GTEC-funded Task B provides for applying TBC systems that were successfully factory-tested in Task A to HP turbine blades. These blades will be made available for piggyback field engine tests. Available field test data will also be used to validate the TBC life models. Design capabilities of the TBC life analysis procedures will be applied to the design analysis of a high-performance thermal-barrier-coated HP turbine component.

Tasks I, IV, and A were active during this reporting period and encompass a literature review, specimen procurement, and data acquisition to calibrate the materials life models. These subjects are reviewed in the following sections.

3.0 TECHNOLOGY ASSESSMENT

To facilitate development of an experimental plan for TBC life prediction, available literature for coating processing, TBC microstructures and composition development, and life prediction were reviewed. Results of this review are presented in the following paragraphs.

3.1 Process-Microstructure Relationships

Two distinct processes have been developed for the application of TBCs to gas turbine components:

- o Plasma Spray
- o EB-PVD

At this stage of development, the plasma-spray process has production status for both combustors and airfoils. In contrast, the EB-PVD process is at an advanced state of development. The following sections review the process-coating microstructure relationships required to achieve viable TBC systems.

3.1.1 Plasma-Sprayed Coatings

The plasma-spray coating process is a form of thermal spray that uses an ionized gas plasma to melt and propel the powdered coating alloy toward the substrate. In this process, a gas mixture is ionized to the plasma state by passing it through a high-intensity electric current. Heat is transferred from the plasma to melt the particles of the injected powdered alloy. Velocity of the plasma can be as high as Mach 2. Powder particles are accelerated by the high velocity plasma and then impacted on the surface of the component to build up the coating.

Plasma-spray factors associated with the degree of particle melting and subsequent particle velocity include the particle size and feed rate, plasma gas composition, electric current strength, and standoff distance to the component. The selection of specific coating parameters depends on the material being sprayed, microstructural requirements, and the equipment design.

The metallic, oxidation-resistant bond coating layer can be applied in either an air environment or a protective atmosphere. The choice is basically dictated by the component metal temperature in service. Application of the oxidation-resistant metallic coating in a low pressure argon environment results in significantly increased oxidation life.

For sheet-metal applications (such as combustors and transition liners), the metal temperature is maintained below about 870C. At these temperatures, air-sprayed NiCrAlY possesses adequate oxidation resistance for long-life applications.

In contrast, turbine airfoils are designed for higher temperature applications above 870C. Consequently, the deposition process should not compromise the oxidation resistance of the bond coating. For this more demanding application, the bond-coating layer is applied using a low pressure plasma spray (LPPS) process in a chamber with a soft vacuum.

The major advantages of LPPS over conventional air plasma spray are better bond strength and oxidation resistance. The better bond strength of LPPS coatings is mainly achieved by the reverse-transfer arc cleaning of the substrate, which removes detrimental base-metal oxides just prior to spraying, and increased substrate temperatures of 870 to 980C, which allow for limited diffusion of the coating into the substrate. In contrast, to avoid excessive oxidation during coating, substrate temperatures in air-plasma spray rarely reach more than 540C.

Ceramic layers of plasma-sprayed TBC systems are typically applied at metal temperatures in the range of 100 to 300C to avoid compressive thermal expansion mismatch stresses, which could buckle the coating.[1] Consequently, mechanical interlocking of the ceramic and metallic layers is the initial adhesion mechanism (Figure 3-1). Thus, a properly applied TBC system has an (Ni,Co)CrAlY/zirconia interface with a high roughness. This interface provides a tortuous path for cracks to follow, and cracks are forced to propagate within the ceramic layer. On the other hand, if the (Ni,Co)CrAlY layer is improperly applied (relatively smooth), the toughness of the interface is low, and zirconia spalling occurs easily at the interface.

The insulative ceramic layer of thermal barrier coatings is usually applied by air-plasma spray. This is necessary to maintain the chemical balance (stoichiometry) of the zirconia, which can become depleted of oxygen if sprayed in a vacuum chamber.

Strain accommodation has been built into plasma-sprayed TBC systems by incorporating 10 to 15 percent porosity into the coating and by using partially stabilized ZrO_2 compositions that produce a large number of subcritical microcracks (Figures 3-2, 3-3). These modifications reduce the apparent elastic modulus and, therefore, minimize the stress that can develop in the ceramic layer for a given strain level. Both of these strain accommodation mechanisms have contributed to the success of plasma-sprayed TBCs. Porosity can be incorporated into virtually all ceramic-layer compositions of interest. Subcritical microcracking is most readily achieved with zirconia partially stabilized with 6 to 8 percent (by weight) of yttria.

Microcracking is not fully developed, however, in the as-sprayed condition. As indicated in Figure 3-3, plasma-sprayed yttria partially stabilized zirconia can develop a columnar solidification structure within most of the "splattered" particle layers. Testing has indicated that thermal cycling is necessary to achieve

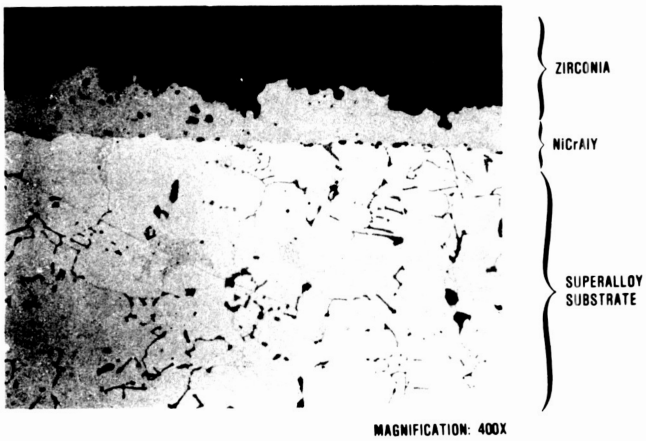

Figure 3-1. A Ceramic-Metal Interface with High Micro-Roughness Maximizes Ceramic Layer Adhesion in Plasma-Sprayed TBCs.

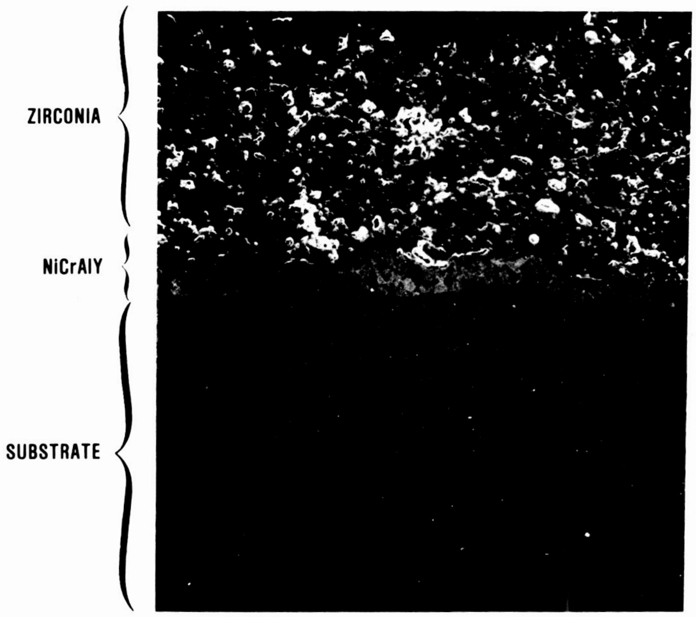

Figure 3-2. The Zirconia Layer of a Plasma-Sprayed TBC System Contains Microporosity and Subcritical Microcracking to Minimize the Elastic Modulus.

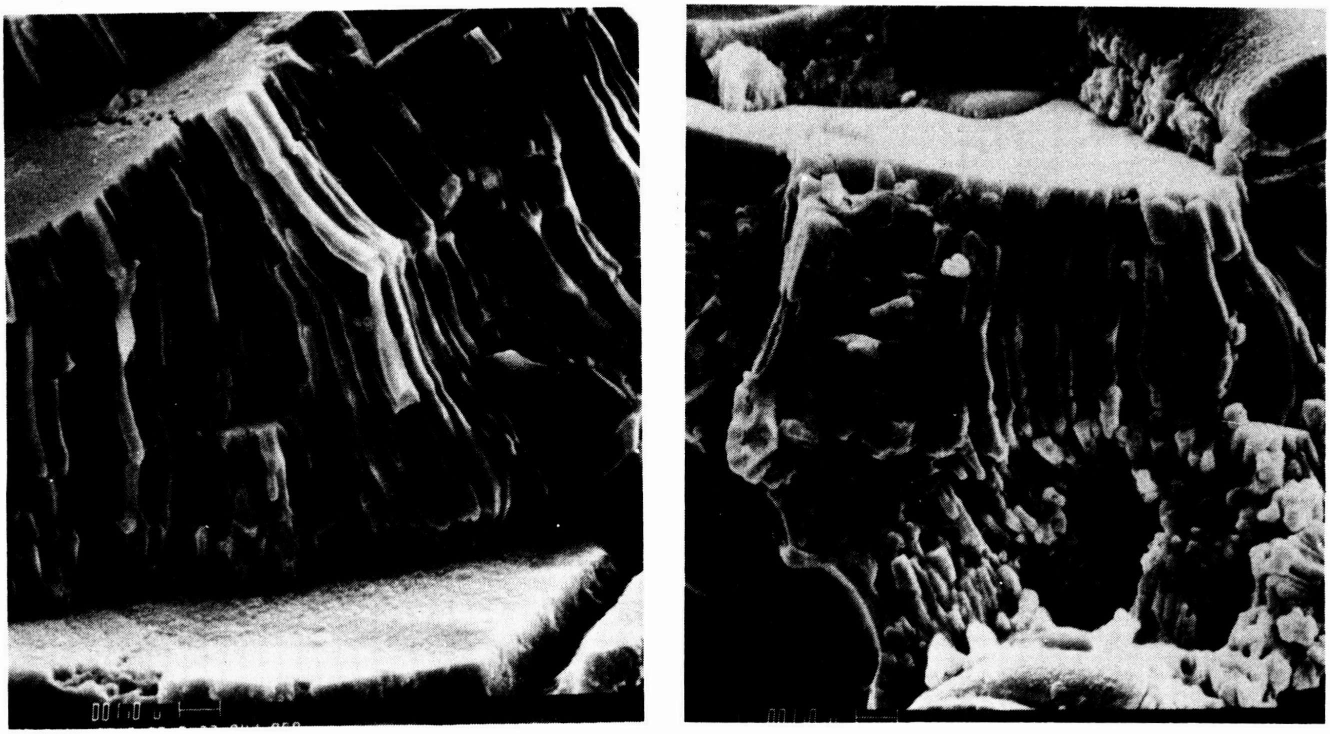

Before Thermal Cycling　　　　After 9000 Oxidation Cycles to 1010°C

Figure 3-3. Localized Columnar Solidification Microstructure in Plasma-Sprayed Zirconia Coating (Partially Stabilized with Yttria) Becomes Microcracked During Thermal Cycling.

the majority of the subcritical microcracking of the solidification microstructure. An acoustic emission study indicated that most of the microcracking probably occurs during the initial thermal cycle(s). Once formed, the small intercolumnar gaps in this microstructure are available to accommodate imposed strains by free expansion (or contraction) of the columns into the gaps, which results in minimal stress build-up in the coating.

Published data[2] indicates that as-sprayed, 8 percent Y_2O_3-stabilized ZrO_2 has tensile and compressive moduli in the 7 to 35 GPa range, which is well below the 154 GPa value for 95 percent dense polycrystalline stabilized zirconia.[3] Following completion of the segmentation of the columnar solidification structure during initial thermal cycling, the elastic modulus of the partially stabilized zirconia may be reduced to well below the levels measured for the as-sprayed coatings.

Acceptable durability of TBCs with strain tolerant microstructures has been thus far limited to relatively mild salt ingestion, mild particulate erosion, and clean fuel environments typical of most aircraft propulsion engine applications. Although zirconia and some other ceramics, such as $ZrSiO_4$, exhibit significant chemical resistance to molten salt attack, thick ceramic coatings will fail mechanically if the salt infiltrates the strain-accommodating porosity and microcracks.[2,4] To alleviate this problem for industrial turbine application, NASA has found that laser glazing of the surface of the zirconia can significantly increase durability of TBCs in the presence of molten salt films.[4] Similarly, Westinghouse has reported that thin glass-rich surface layers also inhibit molten salt damage to TBCs.[2]

Finally, it should be noted that the as-sprayed surface of a TBC is substantially rougher [e.g., 6.3µm (250µ inch)] than metallic surfaces. This level of roughness is acceptable on components with relatively low gas velocities (combustors and transition liners) but adversely affects the aerodynamic performance of turbine blades and vanes. Consequently, airfoils with plasma-sprayed TBCs require some form of media finishing to reduce surface roughness to about 2.5μm (100 μ inch).

3.1.2 EB-PVD Coatings

EB-PVD is the other coating process that has been successfully used to apply TBCs that are viable on gas turbine blades and vanes. Conceptually, this method is a modification of the high-rate vapor deposition process for metallic coatings that has been successfully used to coat millions of turbine airfoils.[5] Power to evaporate the ceramic coating material is provided by a high-energy electron beam gun. Oxygen is also bled into the yttria-stabilized zirconia vapor cloud to minimize any deviations from stoichiometry during coating. This process feature is required since zirconia becomes somewhat oxygen deficient due to partial dissociation during evaporation in a vacuum. Vapor from this cloud condenses onto the turbine airfoil to form the coating.

Unlike the plasma sprayed TBCs, EB-PVD TBCs achieve maximum durability when applied to a smooth, preferably polished, surface.[6] Consequently, this type of coating depends on a chemical bond for adhesion of the ceramic and metallic layers. Higher deposition temperatures in the 870 to 1090C range and/or postcoating heat-treatments in the 980 to 1090C range are typically used to achieve the required bond quality. Clean surfaces that are free of absorbed gases (e.g., water vapor) and loose oxides are also required to obtain an adequate ceramic-to-metal bond during coating.

Ceramic layer microstructure modification for strain accommodation has been most successful with EB-PVD-applied TBC systems. As shown in Figure 3-4, the EB-PVD process has the capability of depositing the ceramic layer with a columnar microstructure with

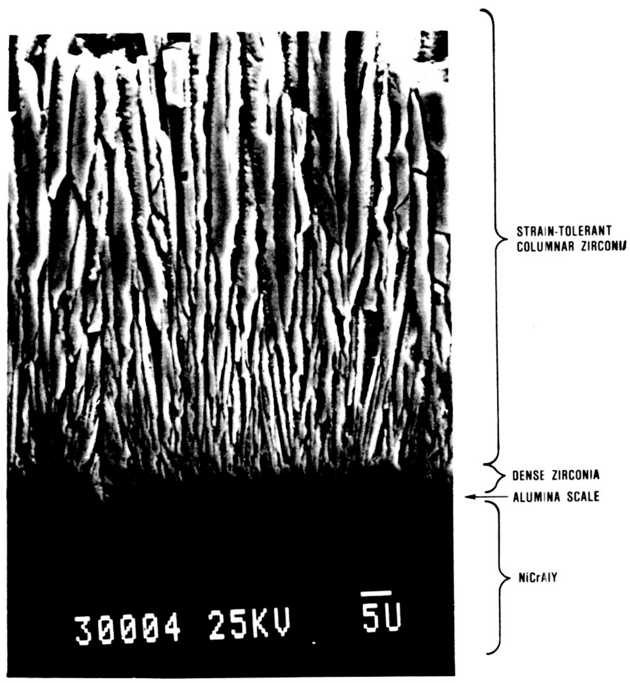

Figure 3-4. EB-PVD-Applied TBC System Has a Strain-Tolerant Columnar Zirconia Microstructure. (Photograph courtesy of Temescal)

intercolumnar structural discontinuities, which results in negligible stress build-up in the zirconia layer of the coating. To illustrate the success of this approach, NiCoCrAlY + 125μm Y_2O_3 (20 percent weight) stabilized ZrO_2 coatings applied to MAR-M 200+Hf specimens have been burner rig tested to more than 29,000 cycles without failure (cycle: 1010C/4 minutes + forced air-cool/2 minutes).[6,7,8]

Close inspection of the ceramic-to-metal interface zone of an EB-PVD applied coating (Figure 3-4) indicates the presence of a thin, dense zirconia layer adjacent to the oxidation inhibiting aluminum oxide scale. This dense layer improves bonding but can develop high compressive stresses during cooling due to the ceramic-metal thermal expansion mismatch. Consequently, thickness of the dense zirconia layer is minimized during deposition to less than about 2 microns to avoid overloading the interface.[5]

The formation of the dense zirconia appears to be associated with the initial deposition of the zirconia in an oxygen-deficient condition, which enhances the development of the bond and the sintering aid effects of transient oxides (e.g., NiO, Cr_2O_3) on the surface of the alumina scale. Once the bond has been established, the oxygen bleed is quickly activated to facilitate the formation of stoichiometric zirconia and the open columnar (low-stress) microstructure.

Erosion resistance of TBC systems is microstructure dependent. A general trend is that denser zirconia coatings are more erosion resistant. Erosion rate data for a medium percent (10 to 15 percent) porosity plasma-sprayed yttria-stabilized zirconia, EB-PVD yttria-stabilized zirconia, and laser-glazed EB-PVD zirconia are illustrated in Figure 3-5. Inspection of this data indicates TBC

ORIGINAL PAGE IS
OF POOR QUALITY

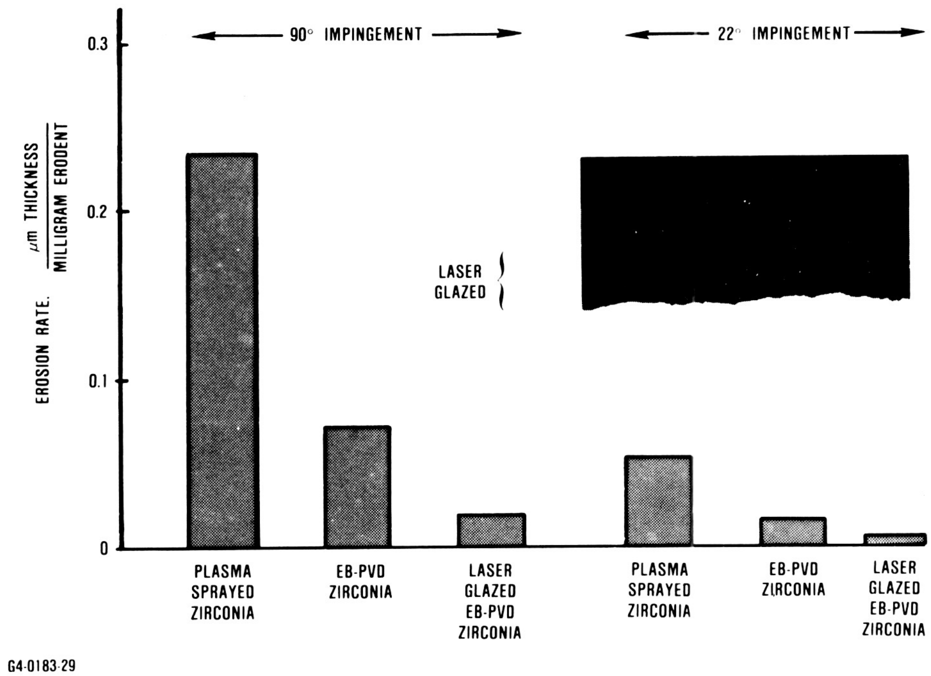

Figure 3-5. TBC Erosion Rates Are Dependent on Zirconia Microstructure and Impingement Angle.

MP-93954

erosion rates are strongly dependent on particle impingement angle and surface condition. Some laser-glazed EB-PVD zirconia coatings have exhibited low rates of erosion.

3.2 TBC Durability and Life Prediction

Durability of a TBC system on gas turbine components in an aircraft engine depends predominantly on the strain tolerance of the ceramic layer, toughness of the ceramic-metal interface, and the oxidation resistance of the metallic bond coating layer.

3.2.1 Thermomechanical Considerations

The effectiveness of the strain-accommodating microstructural features was verified by Sheffler [9] in spalling strain tests. Both plasma-sprayed and EB-PVD applied TBC systems were reported to have a significant strain-tolerant range ($>|\pm 1$ percent$|$ strain) as indicated in Figure 3-6. Examination of the data indicated that the spalling strains for the plasma-sprayed zirconia were not strongly dependent on thickness or temperature. The strain tolerant range for EB-PVD applied zirconia coatings was also greater than those of the plasma-sprayed system. These data indicate that both plasma-sprayed and EB-PVD yttria stabilized zirconia coatings can be applied with sufficient strain tolerance for most gas turbine applications.

Fracture toughness of yttria-stabilized zirconia coatings has been estimated using a double cantilever beam,[2] hardness indentation,[10] and modified bond test methods[11] (Figure 3-7). As indicated in Figure 3-8 for NiCoCrAlY plus EB-PVD yttria-stablized-zirconia coated specimens processed with different conditions, the toughness test provides considerable failure mechanism information in addition to the K_{IC} measurement. The fracture plane, in particular, is clearly identified. Elements present on the fracture surfaces can be quantified by an energy dispersive X-ray (EDX) analysis, and the

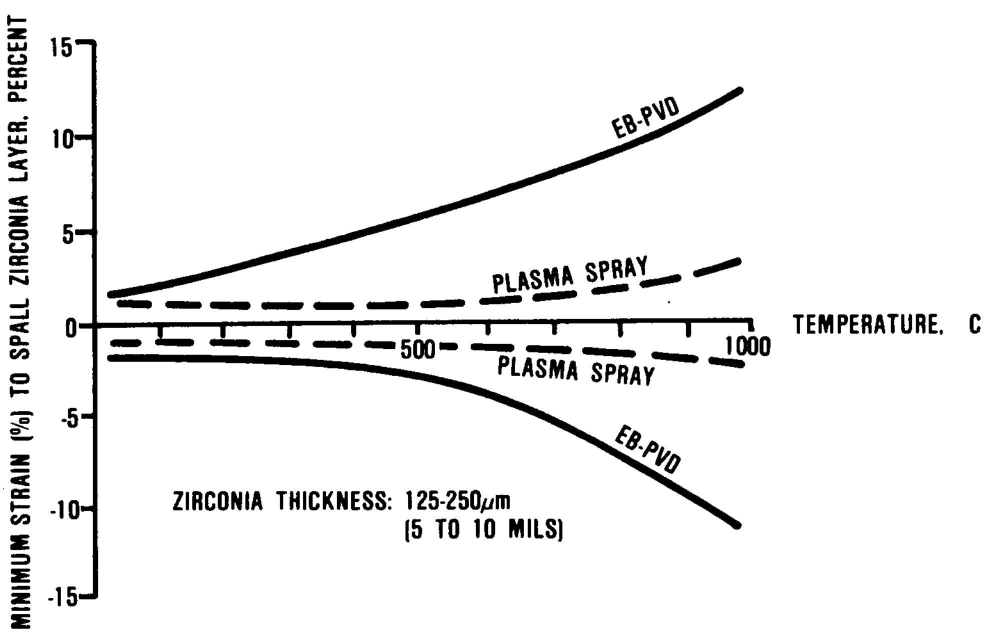

Figure 3-6. Spalling Strains for Thermal Barrier Coatings Are Dependent on Deposition Process and Zirconia Microstructure.[9]

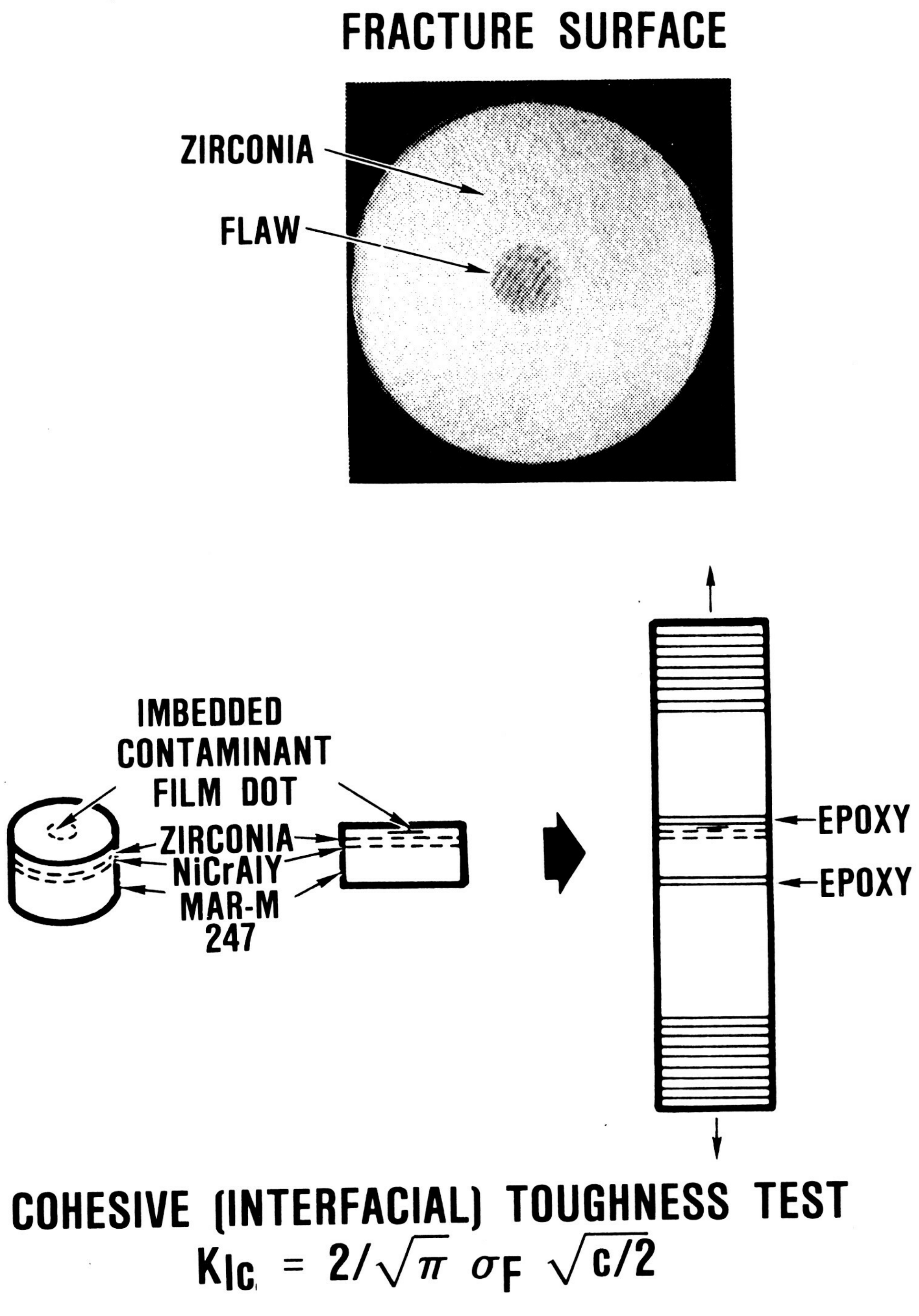

Figure 3-7. Cohesive and Interfacial Toughness of TBC System Can be Quantified with Modified Bond Strength Test.

GARRETT TURBINE ENGINE COMPANY
A DIVISION OF THE GARRETT CORPORATION
PHOENIX, ARIZONA

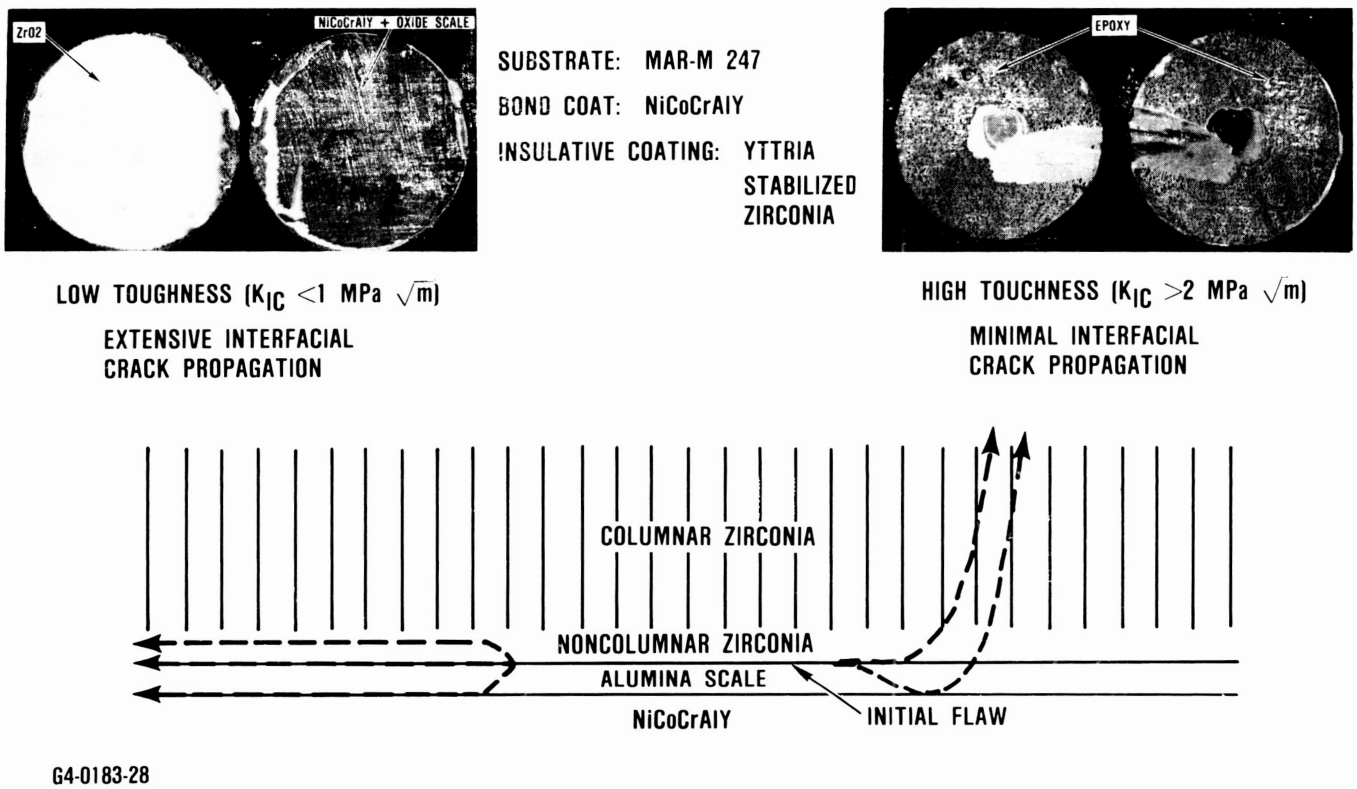

Figure 3-8. Interfacial Toughness Test Identifies Microstructure Weakness and Quantifies Influence of Process Modifications.

fractured microstructure can be examined at high magnifications with SEM. Consequently, the weak point(s) in the system can readily be identified, which facilitates the corrective process or composition adjustments. These tests have yielded toughness values in the range of 0.5 to 3.2 $MPa\sqrt{m}$ for plasma-sprayed yttria (8 weight percent) stabilized zirconia coatings. Interfacial toughnesses of EB-PVD yttria-stabilized zirconia coatings are also within this range. Toughnesses in this range are sufficient for ceramic coating adhesion (and cohesion) provided that the stresses within the zirconia layer are very low; i.e., achieving the low modulus microstructures is critical to a successful application.

As indicated in Figures 3-6 and 3-9, zirconia spalling can be caused by tensile and compressive strains.[9] For TBC-coated components, it has been reported that the most consistent failure mode of the TBC is compressive buckling.[9,11,15]

Zirconia spalling is caused by the complex coating and interface stresses that result from several loading sources. The thermal-mechanical response of the substrate material dominates the coating response. Centrifugal loads and thermal gradients combine to produce a thermal-mechanical response cycle that provides boundary conditions for the zirconia and bond coat response. The coating and interface stresses are further complicated by thermal stresses that develop due to thermal gradients across the coating and the mismatch in thermal expansion between the coating and substrate. The modeling of the coating and interface stresses that drive the failure process requires constitutive data describing the response characteristics of the zirconia, the bond coat, and the substrate. Time-dependent volumetric changes in the coating due to sintering shrinkage and phase transformation can lead to coating-substrate mismatch and additional coating interface stresses.

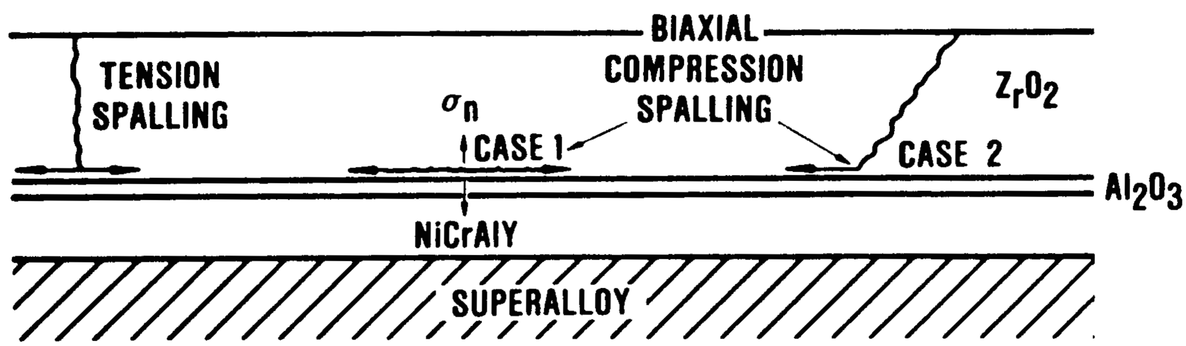

64-0183-19

Figure 3-9. TBCs Have Tensile and Compressive Mechanical Failure Modes.

Andersson, et al., at Westinghouse[2] have attempted to solve the mechanical problem by developing a fracture mechanics approach to analyze the propagation of interfacial cracks to a critical size. Their analysis indicated that TBCs could be predicted to have satisfactory lives in industrial turbines (operating with clean fuels) with low effective values of the zirconia elastic modulus in the order of 7 to 21 GPa.

Measured cyclic crack growth rates parallel to the ceramic-metal interface had a large exponential dependence on the stress intensity factor:

$$\frac{da}{dN} = 153.4\ \Delta K_I^{17.3}$$

where da/dN is the cyclic crack growth rate and ΔK_I is the stress intensity factor in $MPa\sqrt{m}$ for a crack propagating parallel to the interface. For stresses normal to the interface less than 5.5 MPa, lives in excess of 10^4 cycles could be calculated. For slightly higher stresses above 9.0 MPa, one-cycle failures were predicted. (Residual stresses, which can be beneficial,[1] were not considered in this Westinghouse analysis.)

The magnitude of the exponent on the cyclic crack growth rate relationship may preclude reliable fracture mechanics analyses of stable crack growth. If this is the case, the flaw sensitivity of TBCs will require a critical stress intensity factor criterion.

It should be noted that the Andersson analysis is an extension of an earlier TBC life analysis by McDonald and Hendricks.[16] Both of these analytical models assumed that mechanical damage occurred during heat-up in the first few seconds of each cycle. Miller and Lowell[13] tested that hypothesis and concluded that heat-up stresses in a Mach 0.3 burner rig were insufficient to spall a good coating unless oxidation-induced crack growth occurred during prior thermal cycles. Very high heat flux tests conducted by Miller and Berndt[17] also showed that a good coating will not fail on heating unless there has been considerable preoxidation. Prior to this program, however, the possibility of reducing the fracture toughness of a good zirconia coating to significantly lower values as a function of exposure time and temperature has not been investigated. An Andersson type analysis is expected to be valid for TBC systems with low fracture toughness.

3.2.2 Thermochemical Considerations

For TBC systems with adequate strain tolerance, oxidation or molten salt film damage becomes the life-limiting factor.[11,12] Since the zirconia layer is virtually transparent to oxygen, oxidation resistance is provided by the metallic coating layer. Compositions of these coatings are tailored to form thin, adherent, aluminum oxide scales at the boundary between the metallic and ceramic coating layers. This alumina layer grows very slowly and inhibits additional oxidation.

Spalling failures are induced by the kinetics of the breakdown of the oxidation-resistant metallic coating layer and its protective alumina scale. This should not be interpreted to mean that cracking or crack propagation is absent in strain-tolerant TBCs. Spalling necessarily involves the propagation of cracks. The primary difference between strain-tolerant and nonstrain-tolerant TBCs is that the kinetics of crack propagation are controlled by oxidation (time and temperature) in strain-tolerant TBCs. The following two examples illustrate this conclusion.

For plasma-sprayed TBCs, breakdown of the oxidation-resistant bond coating frequently occurs at the high points. One possibility is that when the alumina scale breaks down, other faster growing metallic oxides (e.g., NiO) are produced with additional oxidation. The volumetric expansion of these oxidation products propagates microcracks in the ceramic layer by a wedge open loading mechanism as indicated in Figure 3-10. On subsequent heating, the ceramic layer is thermally isolated from the substrate by the crack. Rapid heating of the unbonded ceramic region results in rapid thermal expansion, which further propagates the microcracks until buckling and spalling occur.[11,13]

For EB-PVD coatings with open columnar microstructures, the stresses on the ceramic-metal interface are primarily dependent on the thickness of a thin, dense ceramic layer adjacent to the metallic layer surface.[5] The alumina scale, which increases in thickness as a function of time and temperature in an oxidizing environment, is included in the dense ceramic layer thickness that loads the ceramic-metal interface (e.g., by ceramic-metal thermal expansion mismatched stresses). Consequently, alumina scale growth will eventually result in ceramic-layer stresses sufficient to overload the interface or sustain crack propagation in the dense ceramic layer adjacent to the interface.

Although both TBC failure mechanisms described have mechanical attributes, the failure rates are controlled by oxidation and, consequently, are time- and temperature-dependent.

Available data in the literature indicates that the oxidation resistance of TBCs applied by the EB-PVD process can be somewhat better than those applied by plasma-spray processes.[6-9,11] Figure 3-11 illustrates this conclusion with the best literature data reported to date as a function of bond coating temperature. The slopes extrapolating the temperature dependence are based on experience with metallic coating oxidation. Other variables that affect TBC life are cycle frequency[12] and bond coating thickness.

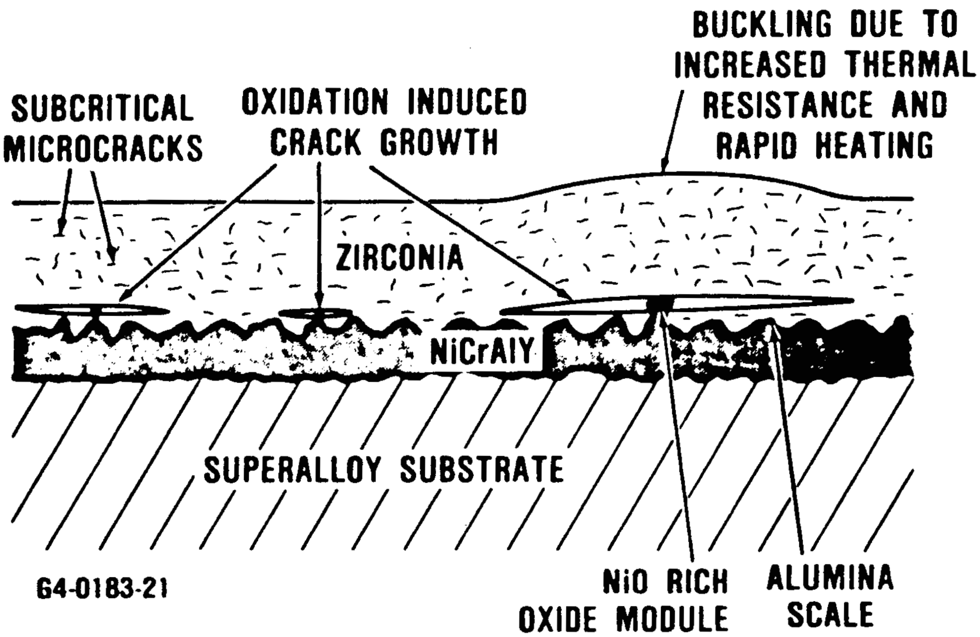

Figure 3-10. Oxidation-Induced Spalling in Plasma-Sprayed TBC.

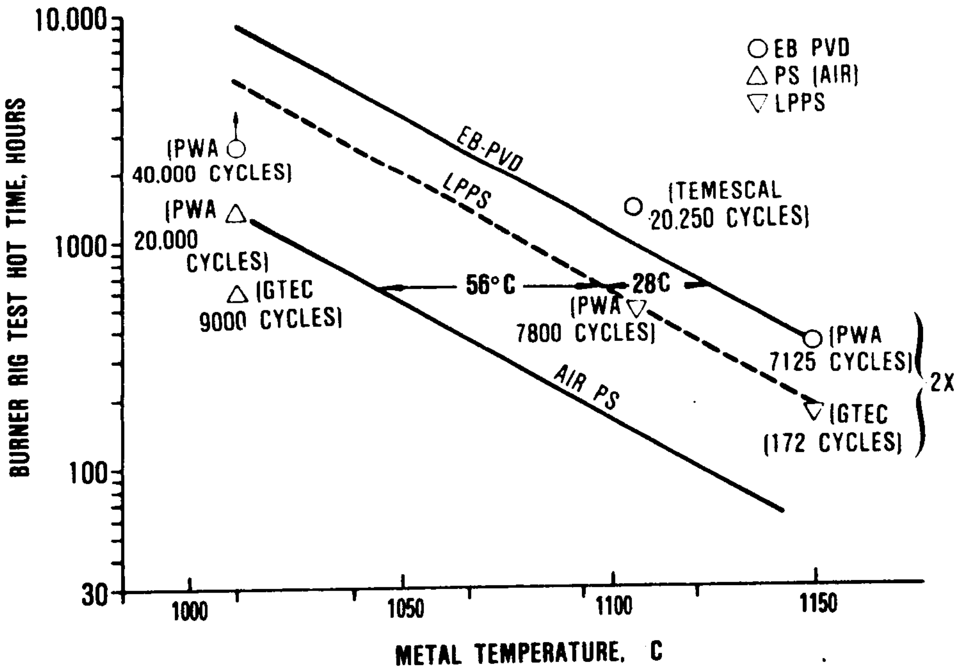

Figure 3-11. TBC Application Process and Temperature Affect the Oxidation Life of the Bond Coating.

One reason for the differences in oxidation resistance is attributable to the plasma-sprayed TBCs requirement for a rough ceramic-metal interface to achieve an adherent, mechanically interlocked TBC system. The very rough ceramic-metal interface significantly increases the surface area requiring protection, compared to the smooth interface of EB-PVD coatings.

Another factor affecting the durability of plasma-sprayed TBCs is the quality of the metallic bond coating layer. In particular, spraying the bond coat in air results in significant oxidation of the aluminum and other reactive elements such as Hf, Y, and Zr, which facilitate adhesion of the alumina scale at the ceramic-metal interface. Consequently, as shown in Figure 3-11, application of the bond coating layer in the relatively clean low-pressure argon environment of the LPPS process can significantly increase oxidation resistance.

To be a viable mission analysis and design tool, thermochemical life prediction models must predict coating durability as a function of engine, mission and materials system factors. GTEC has developed a mechanistic model (Figure 3-12) which predicts oxidation and hot corrosion life of metallic coatings in terms of metal temperature, fuel quality, aircraft altitude (salt ingestion), turbine pressure and velocity.[14] Computer-generated coating lives for a diffusion aluminide coating are provided in Figure 3-13 to illustrate the capability of the model.

A similar approach is anticipated in the development of a thermochemical model for TBC life. In steady-state burner rig tests, simulating industrial turbine conditions, TBC failure conditions have been successfully correlated as a function of condensate melting points and dew points.[18] Although hot corrosion attack of the zirconia is not expected to be significant in an aircraft engine

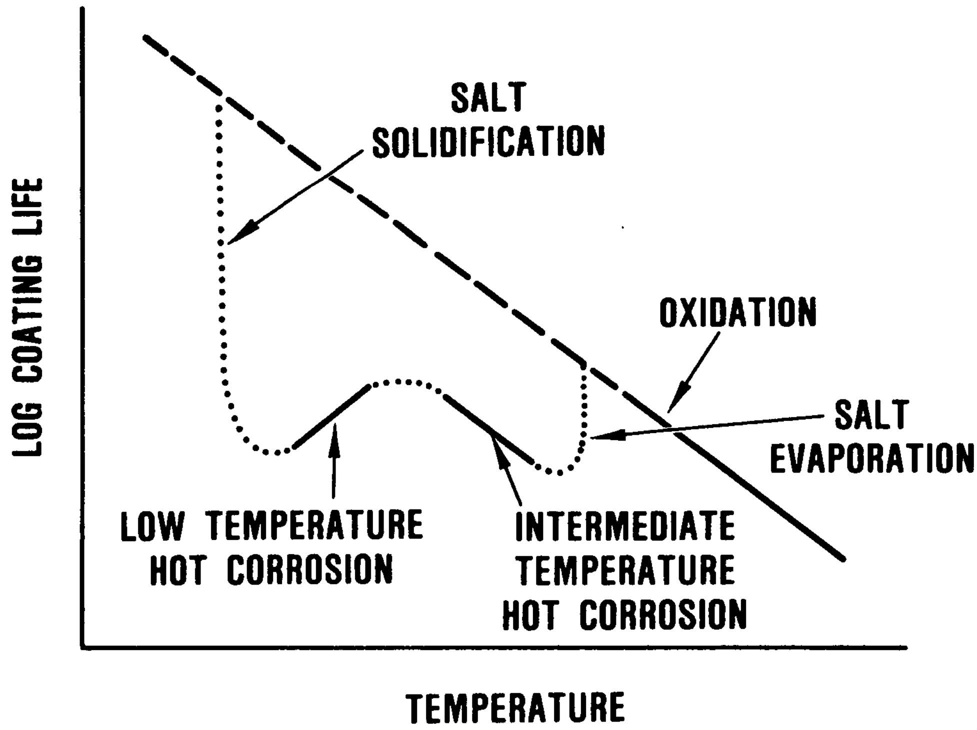

Figure 3-12. Environmental Life Model Incorporates Two Modes of Hot Corrosion and Oxidation.

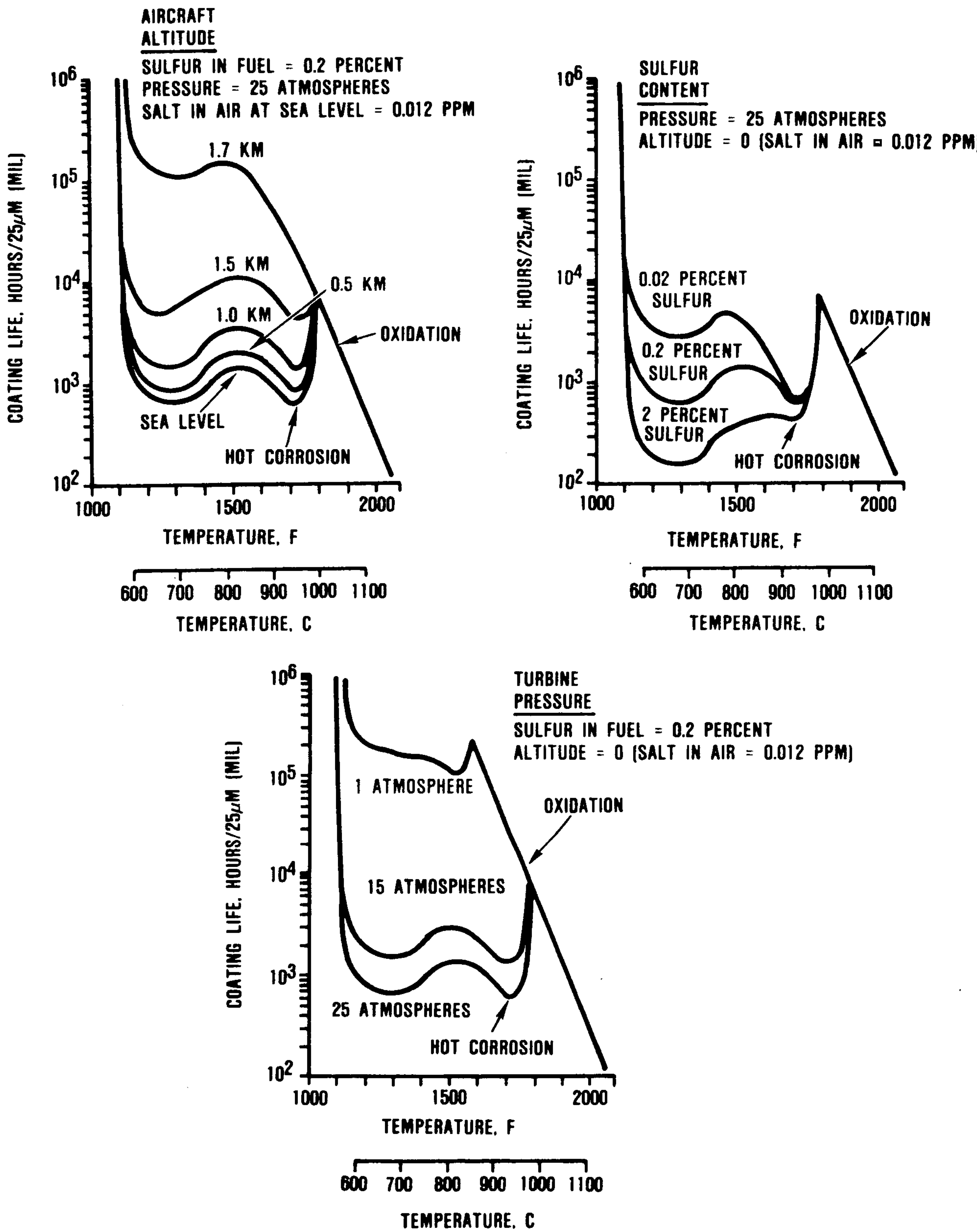

Figure 3-13. Diffusion Aluminide Coating Life Is Predicted By a Computer Model.

environment, molten salt film induced mechanical damage is of concern for some mission environments. Therefore, a salt-film damage function of temperature, pressure, and altitude (salt ingestion) is expected to be incorporated into a thermochemical life model for TBCs. The anticipated shape of the TBC life model is shown in Figure 3-14.

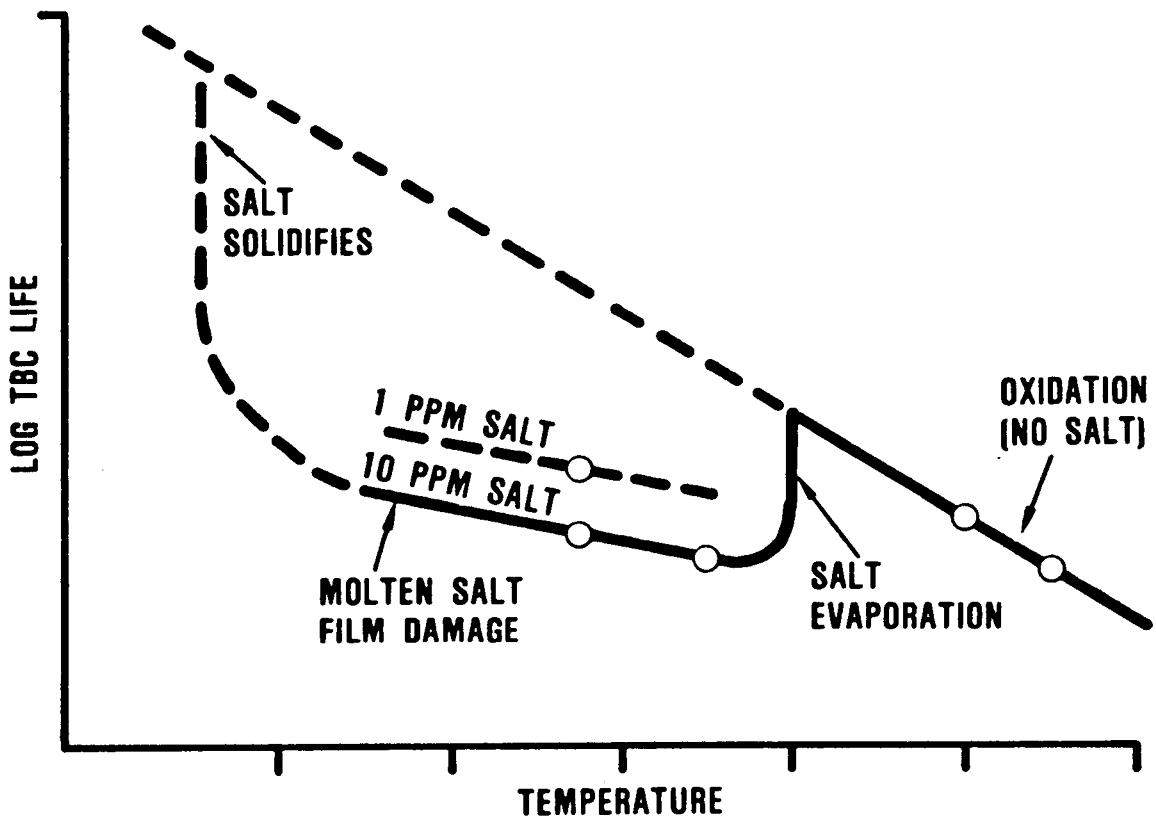

Figure 3-14. Anticipated Thermochemical TBC Life Prediction Model Will Have Oxidation and Molten Salt Film Damage Modes.

4.0 TBC SYSTEMS AND SPECIMEN PROCUREMENT

The objective of this program is to develop life prediction methods for plasma-sprayed and EB-PVD TBC systems. This effort is focused on the following TBC systems applied by three commercial suppliers:

Chromalloy - NiCrAlY (LPPS) + 8 percent Y_2O_3 stabilized ZrO_2 (APS)

Klock - NiCrAlY (LPPS) + 8 percent Y_2O_3 stabilized ZrO_2 (APS)

Temescal - NiCoCrAlY (EB-PVD) + 20 percent Y_2O_3 stabilized ZrO_2 (EB-PVD)

Compositions and microstructures of these TBC systems are reviewed in the following paragraphs.

LPPS and air plasma-spray (APS) processes were used to apply the Ni-31Cr-11Al-0.5Y oxidation-resistant bond coating and insulative Y_2O_3 (8 percent) partially stabilized zirconia layers of the TBC system, respectively. Specimens were coated using the fixed (proprietary) processes of Chromalloy Research and Technology in Orangeburg, New York and Klock in Manchester, Connecticut. Microstructures of the Chromalloy and Klock plasma-sprayed TBC systems are provided in Figures 4-1 and 4-2.

EB-PVD coatings were applied by Temescal in Berkeley, California using their established (proprietary) fixed process. The EB-PVD TBC system featured a columnar grained EB-PVD applied yttria (20 percent) fully stabilized cubic zirconia insulative layer on top of a Ni-23Co-18Cr-11Al-0.3Y EB-PVD oxidation resistant bond coating. The microstructure of the EB-PVD TBC system is provided in Figure 4-3.

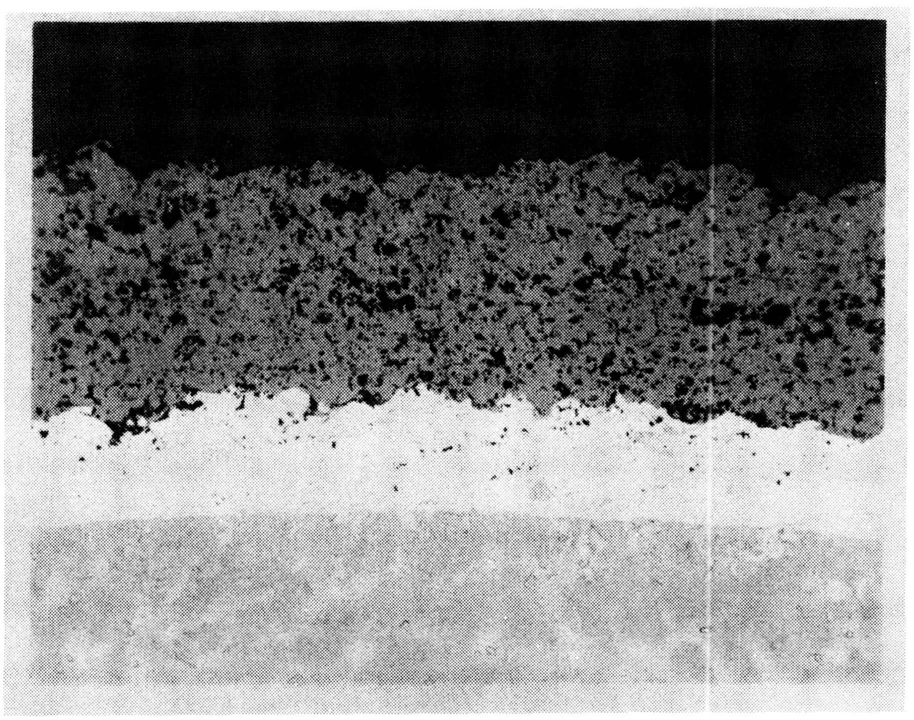

Figure 4-1. Pretest Microstructure of Chromalloy Plasma-Sprayed Ni-31Cr-11Al-0.5Y Plus Y_2O_3 (8 Percent) Stabilized ZrO_2 Thermal Barrier Coating System.

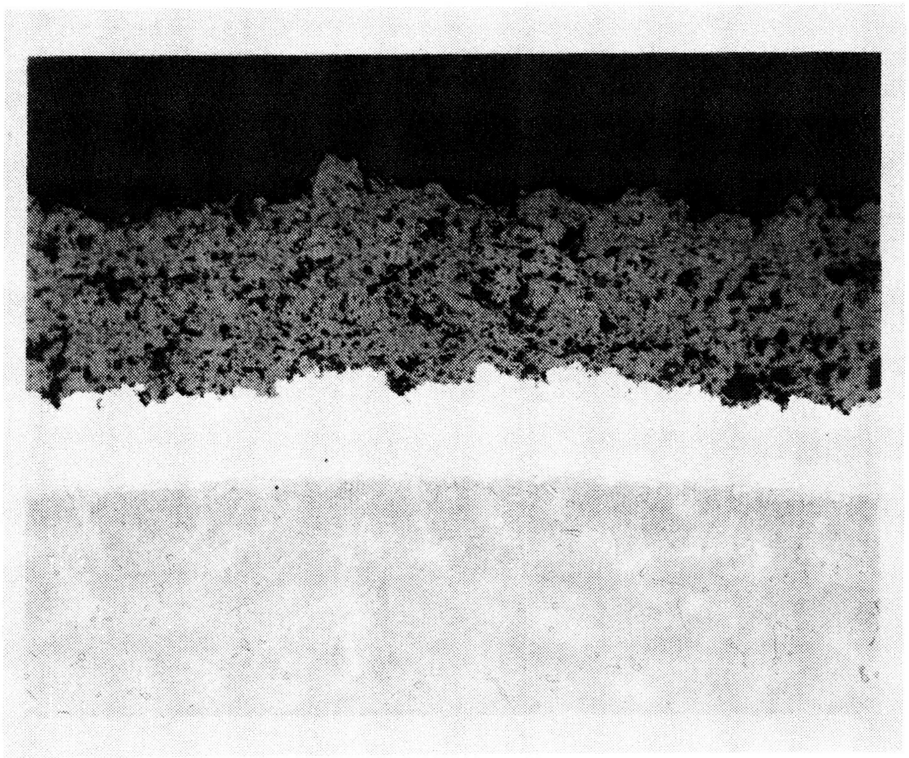

Figure 4-2. Pretest Microstructure of Klock Plasma-Sprayed Ni-31Cr-11Al-0.5Y Plus Y_2O_3 (8 Percent) Stabilized ZrO_2 Thermal Barrier Coating System.

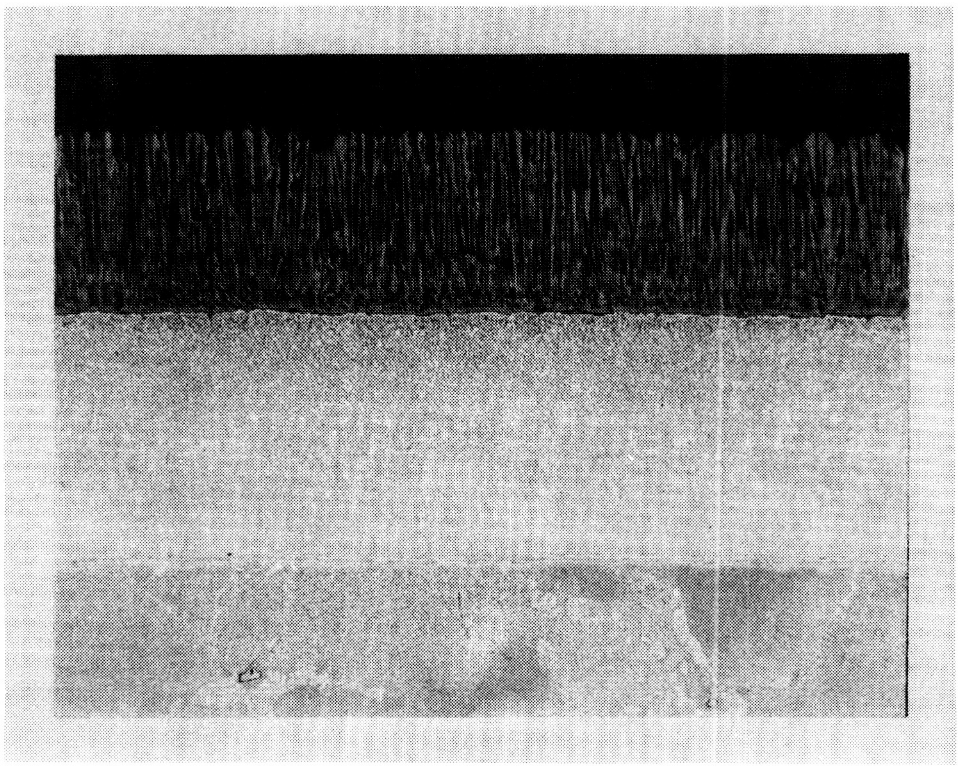

Figure 4-3. Pretest Microstructure of Temescal EB-PVD Ni-23Co-18Cr-11Al-0.3Y Plus Y_2O_3 (20 Percent) Stabilized ZrO_2 Thermal Barrier Coating System.

Capabilities of these TBC systems are being established on specimens machined from MAR-M 247 superalloy castings and IN-718 seamless tubing. Compositions of these alloys are provided in Table 4-1. The cast MAR-M 247 superalloy, which is used in the equiaxed and directionally solidified conditions for turbine airfoils, was selected for all specimens requiring long exposures at elevated temperatures. Burner rig, cohesive (interfacial) strength and toughness, and thermal conductivity specimens were machined from the MAR-M 247 alloy and are shown in Figures 4-4, 4-5, and 4-6, respectively. The cohesive strength specimen was also used for evaluating nondestructive evaluation (NDE) feasibility. Tension and compression spalling strain specimens were machined from the IN-718 alloy and are shown in Figure 4-7.

TABLE 4-1. SUPERALLOY COMPOSITIONS (WEIGHT PERCENT)

	Mo	W	Ta	Cb	Al	Ti	Cr	Co	Fe	Hf	Zr	C	B	Ni
MAR-M 247	0.65	10.0	3.3	--	5.5	1.05	8.4	10.0	--	1.4	0.055	0.15	0.015	Balance
IN-718	3.0	--	--	5.1	0.6	0.9	18.5	--	18.0	--	--	0.04	--	Balance

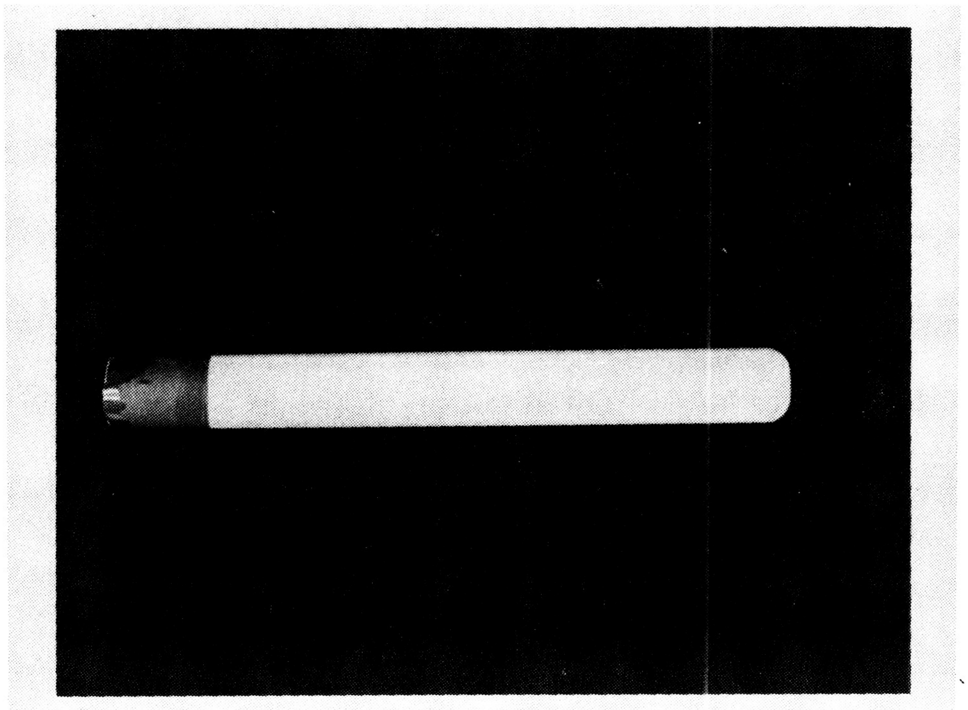

Figure 4-4. Burner Rig Specimens Are Used to Calibrate Environmental Life Model.

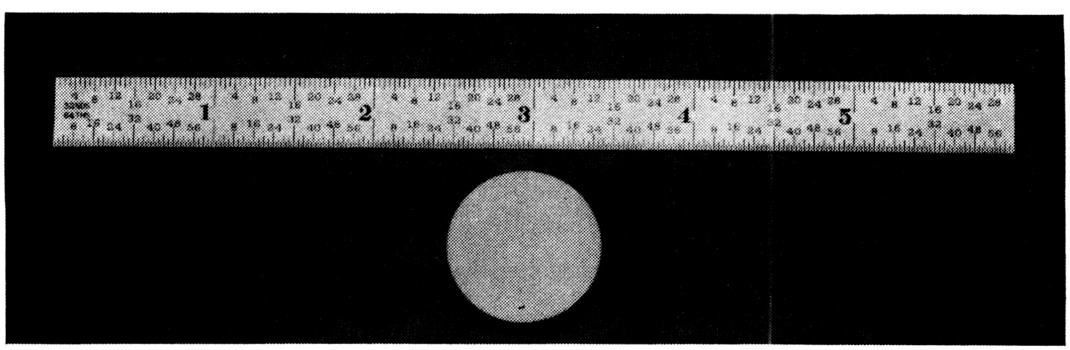

Figure 4-5. Cohesive (Interfacial) Strength and Toughness Specimen Is Used to Obtain Fracture Mechanics Data. This Specimen Is Also Used for NDE Feasibility Studies.

ORIGINAL PAGE IS
OF POOR QUALITY

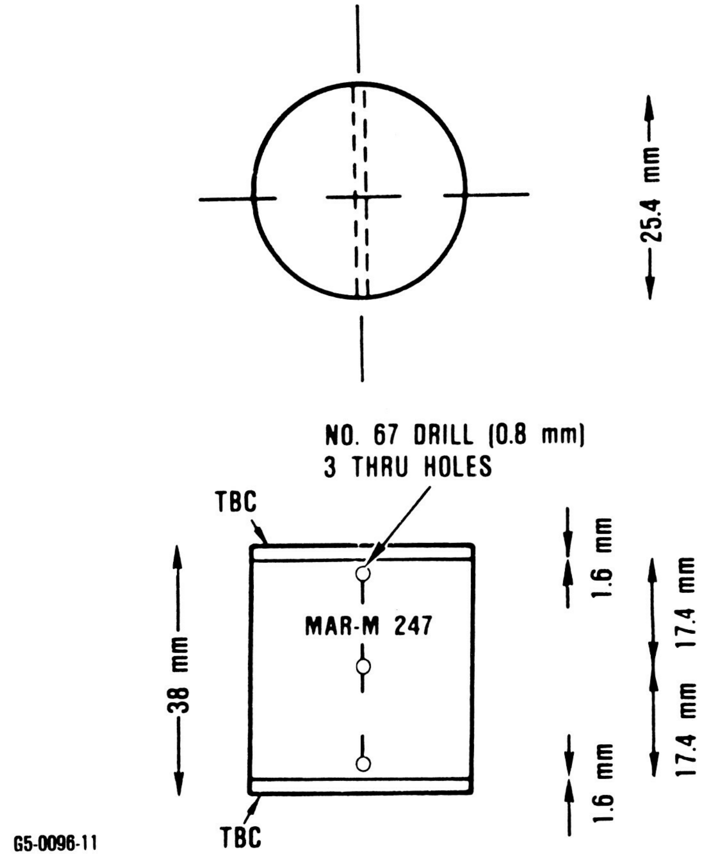

Figure 4-6. Thermal Conductivity Specimens Are Used to Quantify Heat Conductance of Thermal Barrier Coating System.

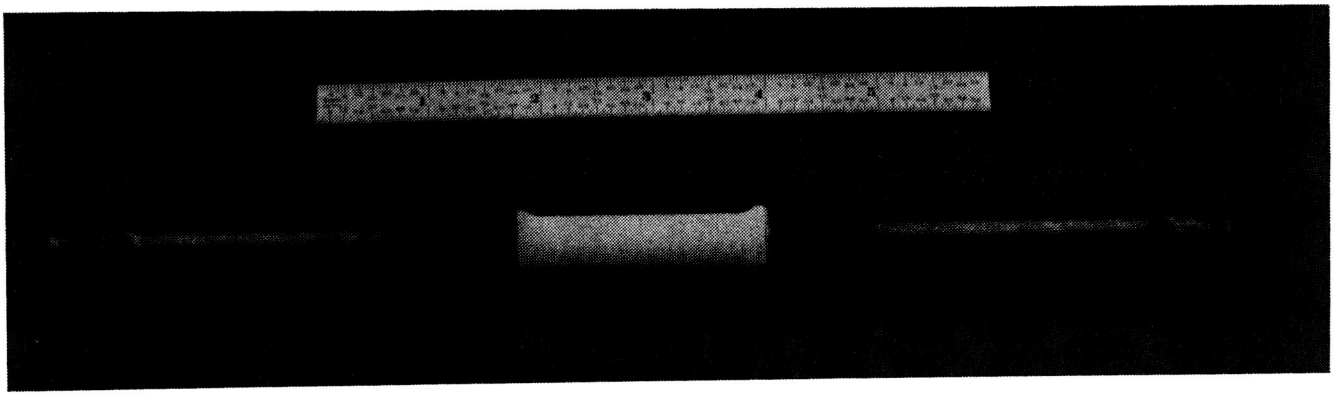

Figure 4-7. Thin-Walled Tube Specimens Are Used to Measure Zirconia Modulus and Spalling Strains in Tension and Compression.

5.0 TBC SYSTEM CHARACTERIZATION

In preparation for the development of thermomechanical and thermochemical models for TBC life, the TBC systems are being characterized for strength and toughness, tensile and compressive spalling strains, oxidation and molten salt film damage, and thermal conductivity. In addition, feasibility is being assessed for NDE methods to quantify TBC thickness, flaw sizes and insulative capability. The status of these investigations is reviewed in the following paragraphs.

5.1 TBC Strength and Toughness

As noted in Section 3.0 (Figures 3-7 and 3-8), a bond strength test can be modified with an artificial flaw in the zirconia or at the zirconia-bond coating interface to yield fracture mechanics data and the cohesive or interfacial strength. Consequently, the objectives of these tests are to characterize the fracture strength, toughness, and effective flaw sizes for the Chromalloy, Klock, and Temescal TBC systems. These TBC properties are being characterized for specimens in the as-received condition, after initial thermal cycling (three 10-minute exposures to 1000C followed by air cooling) and after extended exposures in a high temperature oxidation environment (e.g., up to 60 hours at 1150C and up to 600 hours at 1100C). Results of tests performed thus far are reviewed below.

Cohesive strength data for the plasma-sprayed zirconia were obtained by epoxy bonding TBCed bond specimens (Figure 3-7) into threaded pull rods and loading to fracture in a universal tensile test machine. Fracture toughness of the zirconia was obtained by incorporating an artificial (vacuum grease) flaw of known diameter into the coating and testing in a similar manner. The fracture toughness relationship for a penny-shaped crack in an infinite body subjected to uniform tension,

$$K_{Ic} = 2/\sqrt{\pi}\ \sigma_f \sqrt{c/2} \qquad \text{Equation (1)}$$

where σ_f is the fracture strength of the flawed specimen and c is the flaw diameter, was used to estimate the fracture toughness of the yttria partially stabilized zirconia layer.

The Chromalloy cohesive toughness specimens failed as expected at the artificial flaw as shown in Figure 3-7. Cohesive strength specimens failed in the zirconia just above the NiCrAlY bond coating (Figure 5-1) or in the epoxy at higher failure stresses. Average values for fracture toughness, cohesive strength, and effective flaw sizes calculated from Equation 1 are provided in Table 5-1 for the Chromalloy TBC system.

These tests indicated that thermal cycling increased the fracture toughness (Figure 5-2) and cohesive strength of the zirconia. Microstructures and fracture surfaces are being examined with the scanning electron microscope (SEM) and X-ray diffraction to determine if the increase in toughness is associated with microcracking or phase transformations.

Cohesive strength and toughness of the zirconia layer of the Chromalloy TBC system has also been measured as a function of exposure time at 1150C. As indicated in Figure 5-3 and Table 5-2, exposures of 10 to 60 hours at 1150C reduced the zirconia toughness. Visual examination indicated that the cracks in the toughness specimens propagated within the zirconia. Posttest examination of these specimens is in progress.

GARRETT TURBINE ENGINE COMPANY
A DIVISION OF THE GARRETT CORPORATION
PHOENIX, ARIZONA

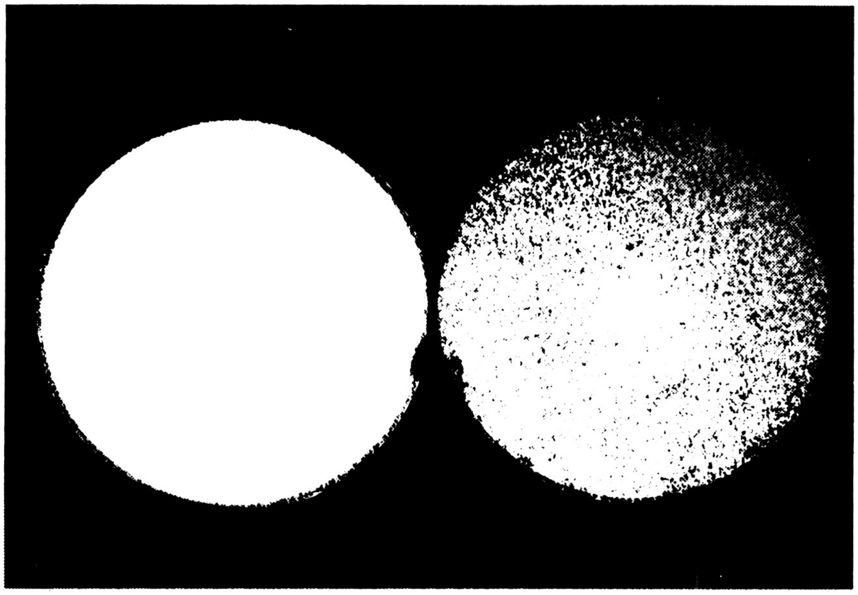

G5-0096-4

EFFECTIVE FLAW SIZE IS ≤1 mm

$$c = \frac{\pi}{2}\left(\frac{K_{Ic}}{\sigma_f}\right)^2 \leq 1\,mm$$

Figure 5-1. Cohesive Strength Failures of Chromalloy TBC System Occur Adjacent to the NiCrAlY-Zirconia Interface.

TABLE 5-1. COHESIVE STRENGTH AND TOUGHNESS OF CHROMALLOY PLASMA-SPRAYED TBC SYSTEM

SPECIMEN IDENTIFICATION	1000C CYCLED	THERMAL EXPOSURE TEMP, C	THERMAL EXPOSURE TIME, HR	FAILURE STRESS, MPa	ARTIFICIAL FLAW SIZE, mm	K_{Ic}, MPa$\sqrt{m}$	CALCULATED CRITICAL FLAW SIZE, mm	COMMENTS
C10K0-24	NO	—	—	18.9	0	—	1.2	
C10K0-25	NO	—	—	19.8	0	—	1.1	
C10K0-26	NO	—	—	21.4	0	—	0.9	
C10K3-1	NO	—	—	12.7	3.0	0.55	—	
C10K3-2	NO	—	—	11.3	3.0	0.49	—	
C10K3-3	NO	—	—	12.8	2.5	0.51	—	
C10K6-25	NO	—	—	17.0	5.0	0.96	—	CRACK PATH TURNED DOWN ALONG BOND COAT INTERFACE.
C10K6-26	NO	—	—	16.7	5.0	0.94	—	SAME AS C10K6-25
C10K6-27	NO	—	—	9.5	5.0	0.53	—	
C10K0-21	YES	—	—	23.7	0	—	<1.7	EPOXY FAILURE
C10K0-22	YES	—	—	21.3	0	—	<2.2	EPOXY FAILURE
C10K0-23	YES	—	—	27.2	0	—	<1.3	EPOXY FAILURE
C10K3-4	YES	—	—	15.3	2.5	0.61	—	
C10K3-5	YES	—	—	17.0	2.5	0.68	—	
C10K3-6	YES	—	—	8.6	2.8	0.36	—	
C10K6-21	YES	—	—	16.3	5.0	0.92	—	
C10K6-22	YES	—	—	20.7	5.5	1.22	—	
C10K6-23	YES	—	—	16.8	4.9	0.94	—	

GARRETT TURBINE ENGINE COMPANY
A DIVISION OF THE GARRETT CORPORATION
PHOENIX, ARIZONA

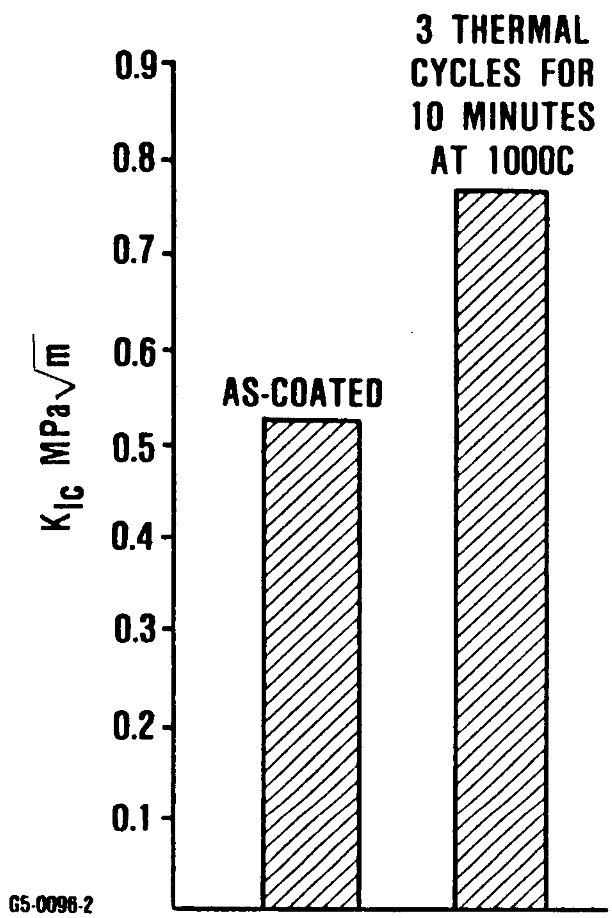

Figure 5-2. Cohesive Toughness of Chromalloy Plasma-Sprayed Zirconia Is Increased by Thermal Cycling.

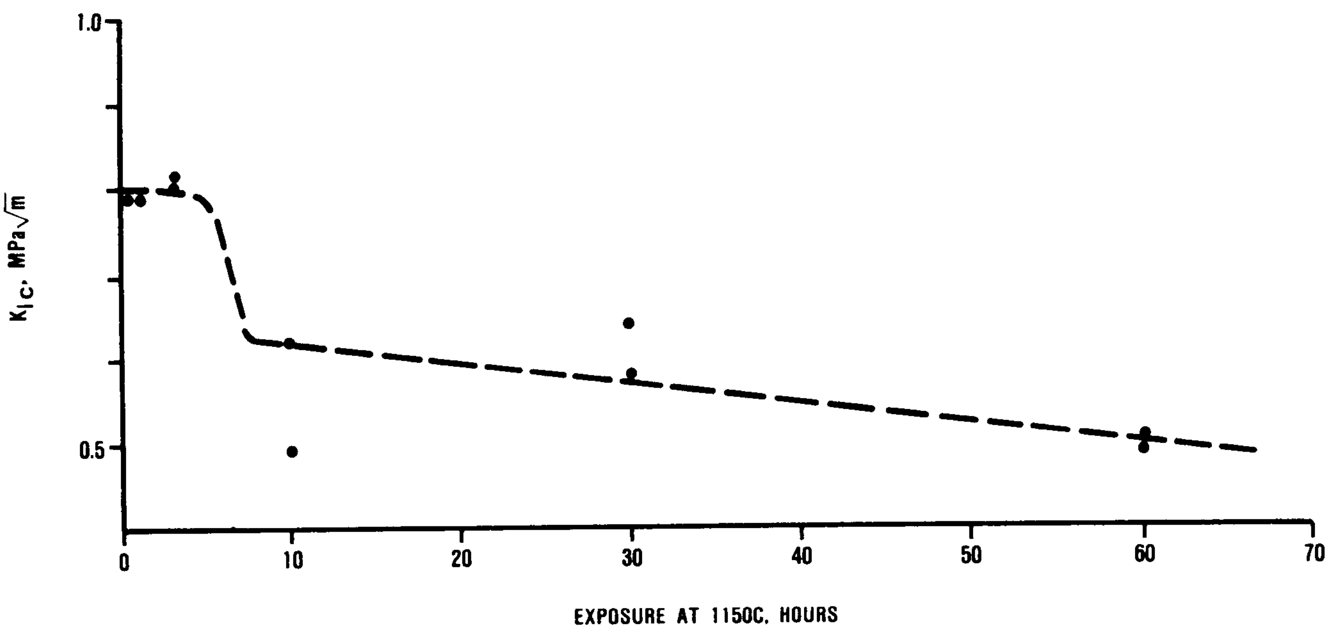

Figure 5-3. Cohesive Toughness of Chromalloy Plasma-Sprayed Zirconia Is Reduced by 1150C Exposure.

TABLE 5-2. COHESIVE STRENGTH AND TOUGHNESS OF CHROMALLOY PLASMA-SPRAYED TBC SYSTEM AFTER AN 1150C EXPOSURE

SPECIMEN IDENTIFICATION	1000C CYCLED	THERMAL EXPOSURE TEMP, C	TIME, HR	FAILURE STRESS, MPa	ARTIFICIAL FLAW SIZE, mm	K_{Ic}, MPa$\sqrt{m}$	CALCULATED CRITICAL FLAW SIZE, mm	COMMENTS
C10K0-11	NO	1150	60	22.1	—	—	0.78	
C10K0-12	NO	1150	60	25.1	—	—	0.61	
C10K0-13	NO	1150	30	22.9	—	—	<1.11	EPOXY FAILURE
C10K0-14	NO	1150	30	28.0	—	—	<0.74	EPOXY FAILURE
C10K0-15	NO	1150	10	32.0	—	—	<0.48	EPOXY FAILURE
C10K0-16	NO	1150	10	28.7	—	—	<0.60	EPOXY FAILURE
C10K0-17	NO	1150	3	31.3	—	—	<1.04	EPOXY FAILURE
C10K0-18	NO	1150	3	32.0	—	—	<1.01	EPOXY FAILURE
C10K0-19	NO	1150	1	20.1	—	—	<2.4	EPOXY FAILURE
C10K0-20	NO	1150	1	32.7	—	—	<2.1	EPOXY FAILURE
C10K6-11	NO	1150	60	8.6	5.0	0.49	—	
C10K6-12	NO	1150	60	8.7	5.0	0.50	—	
C10K6-13	NO	1150	30	10.3	5.0	0.58	—	
C10K6-14	NO	1150	30	11.3	5.0	0.64	—	
C10K6-15	NO	1150	10	8.7	5.0	0.49	—	
C10K6-16	NO	1150	10	10.9	5.0	0.62	—	
C10K6-17	NO	1150	3	14.4	5.0	0.81	—	
C10K6-18	NO	1150	3	14.1	5.0	0.80	—	
C10K6-19	NO	1150	1	19.3	5.0	0.79	—	
C10K6-20	NO	1150	1	19.7	5.0	0.79	—	

In contrast, the initial cohesive strength and toughness tests of the Klock TBC system yielded little useful data. Due to the higher amount of interconnected porosity in the Klock specimens, the epoxy wicked to the NiCrAlY-zirconia interface for specimens bonded equivalently to the Chromalloy specimens. Subsequent efforts to seal the surface of the Klock specimens with a thin epoxy layer before bonding to the pull rods or increasing the viscosity (hardener content) of the epoxy were also unsuccessful; these latter efforts yielded low stress failures that initiated in the epoxy. Further testing of Klock cohesive strength and toughness specimens is being suspended until the epoxy wicking problem can be resolved.

Adhesive strength tests of Temescal's system have also been performed. Thus far, the adhesive strength of the zirconia-NiCoCrAlY coating interface has exceeded the strength of the epoxy. Epoxy failures stresses for fourteen specimens ranged from 27.1 to 38.8 MPa.

5.2 Tension/Compression Spalling Strain Tests

Tension and compression tests of the Chromalloy TBC system has been initiated to quantify tension and compression spalling strains. Preliminary test data are provided in Table 5-3.

Thus far, the tensile test results indicate that the zirconia can experience substantial strain (up to 4 percent) and tensile cracking without spalling at room temperature. As shown in Figure 5-4, spalling of the zirconia did not occur even when the substrate failed.

Zirconia spalling and buckling of the 10-mil-thick tube wall have occurred approximately concurrently in initial compression testing. In all instances, specimen failure strains have exceeded 0.8 percent strain in compression. Compression failure of one specimen did not occur until a strain of 3.1 percent had been obtained (Figure 5-5).

TABLE 5-3. ZIRCONIA SPALLING STRAIN LIMITS OF CHROMALLOY TBC SYSTEM ARE BEING ESTABLISHED

SPECIMEN IDENTIFICATION	ZIRCONIA THICKNESS	1000C CYCLED*	ZIRCONIA SPALLING STRAIN TENSION, PERCENT	ZIRCONIA SPALLING STRAIN COMPRESSION, PERCENT	COMMENT
C10RS-6	250μm	NO	>4.0	—	TENSILE CRACKING IN TBC, BUT NO ZIRCONIA SPALLING.
C10RS-8	250μm	NO	>4.0	—	TENSILE CRACKING IN TBC, BUT NO ZIRCONIA SPALLING.
C10RS-10	250μm	NO	>3.8	—	TENSILE CRACKING IN TBC, BUT NO ZIRCONIA SPALLING.
C10RS-2	250μm	NO	—	1.60	SUBSTRATE BUCKLING AND ZIRCONIA SPALLING.
C10RS-5	250μm	NO	—	0.85	SUBSTRATE BUCKLING AND ZIRCONIA SPALLING
C10RS-7	250μm	NO	—	3.1	SUBSTRATE BUCKLING AND ZIRCONIA SPALLING
C10RS-9	250μm	YES	>4.0	—	TENSILE CRACKING IN TBC, BUT NO ZIRCONIA SPALLING
C0RS-1	0	YES	0.76	—	SPECIMEN FAILURE.
C5RS-2	125μm	YES	>2.0	—	TENSILE CRACKING IN TBC, SPECIMEN FAILURE, BUT NO ZIRCONIA SPALLING.
C5RS-3	125μm	YES	>1.0	—	TENSILE CRACKING IN TBC, SPECIMEN FAILURE, BUT NO ZIRCONIA SPALLING.
C15RS-2	375μm	YES	>1.5	—	TENSILE CRACKING IN TBC, SPECIMEN FAILURE, BUT NO ZIRCONIA SPALLING.

ALL SPECIMENS HAVE A 125μm Ni-31Cr-11Al-0.5Y BOND COATING.

*THREE 10-MINUTE CYCLES TO 1000C

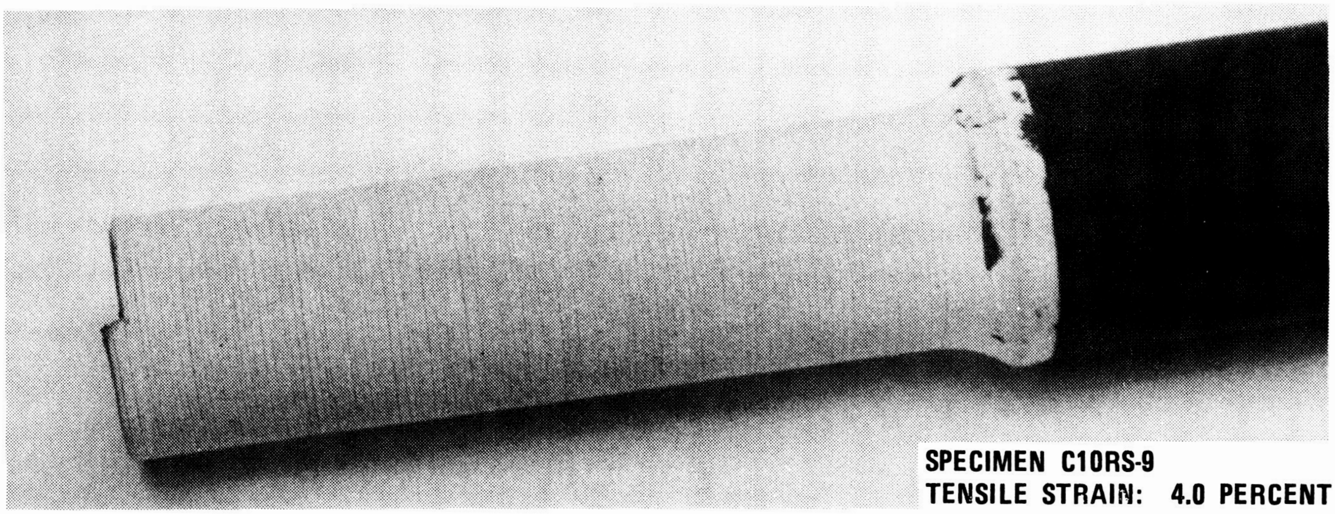

Figure 5-4. Zirconia Layer of Chromalloy TBC System Did Not Spall When the Specimen Failed. Numerous Parallel Tensile Cracks Were Observed in the Zirconia.

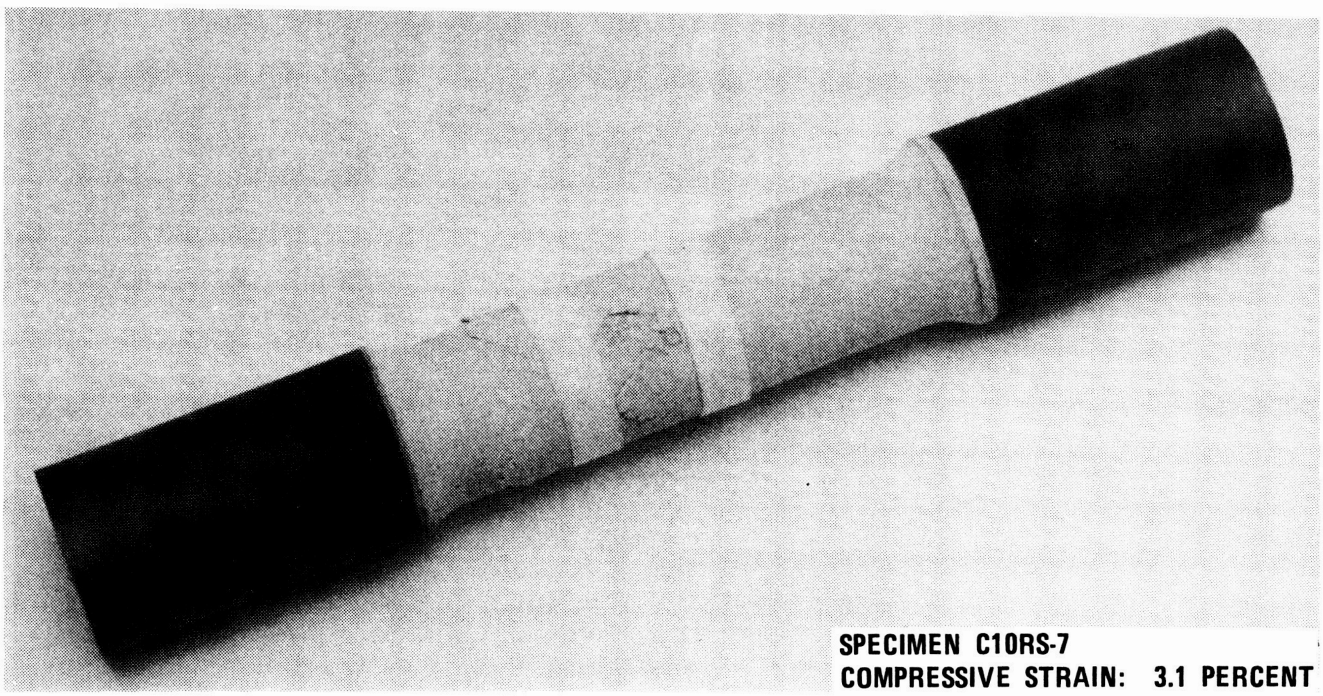

Figure 5-5. Compression Spalling and Substrate Buckling Occurred Approximately Concurrently.

Based on a previous study by Sheffler et al.,[9] spalling strains exceeding 2 percent at room temperature were unexpected.

5.3 Environmental Tests

Burner rig tests to calibrate the thermochemical TBC life model (Figure 3-14) have been initiated. The following two tests are in progress:

- o 1150C cyclic oxidation
- o 925C with 10 ppm sea salt

Duplicate specimens of each TBC system are being concurrently evaluated in each test.

5.4 Thermal Conductivity

Insulative capability of a TBC system and the amount of thermal strain within the zirconia layer requires that the thermal conductivity of the insulative layer be well characterized. Thermal conductivity data available in the literature for yttria-stabilized zirconia vary by about one-half order of magnitude, which is unacceptable for design analyses. Consequently, thermal conductivity data is being obtained for TBCs applied by Chromalloy, Klock, and Temescal. Thermal conductivity measurements are currently being performed on the Chromalloy and Klock plasma-sprayed TBC systems at Dynatech in Cambridge, Massachusetts. Data is being obtained at 500, 800, and 1000C.

5.5 Nondestructive Evaluation Technologies

Feasibility for advanced nondestructive evaluation (NDE) technologies is being assessed to ensure TBC reproducibility and support the application of thermomechanical life prediction models. Candidate techniques being evaluated in this program include:

- o Eddy current

- o Photothermal radiometric imaging (Dr. I. Kaufman, Arizona State University)

- o Scanning photoacoustic microscopy (Dr. R. Thomas, Wayne State University)

These technologies are being evaluated for their capability to quantify zirconia thickness, flaw size, and insulative capability.

Disk specimens (Figure 4-5) coated with the Chromalloy TBC system have been evaluated with the eddy current technique. Results from thickness measurements indicate that variations of about 25 to 50μm in the zirconia thickness will be detectable. The eddy current inspection output of the x-y plotter for the Chromalloy specimens is shown in Figure 5-6. The lines indicate the motion along the liftoff curve of the operating point as the probe is lowered to the surface. Scatter of the end points of the liftoff curves for all the Chromalloy NDE specimens is shown in Figure 5-7. Five points were taken for each specimen along with air and the uncoated back of each specimen. From these results, the present eddy current technique is clearly capable of zirconia thickness determination with resolution to about 25 to 50μm.

Evaluation of the other NDE techniques will occur during the second year of this program.

5.6 Factory Engine Test

TFE731-5 high-pressure turbine blades have been coated with each of the program TBC systems. These blades will be "piggyback" tested in a TFE731 turbofan factory engine to provide data to verify life prediction model accuracy.

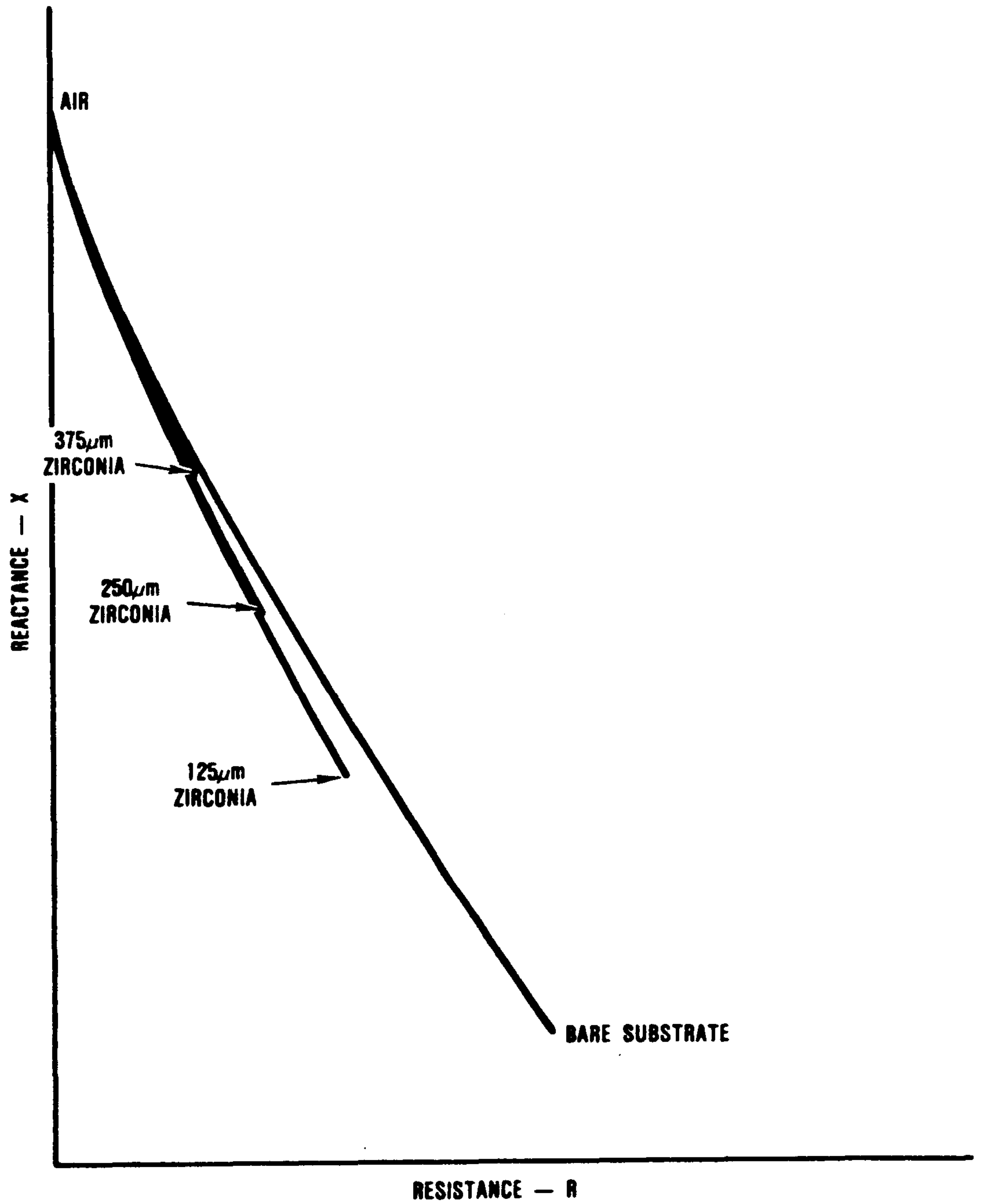

Figure 5-6. Variation of Resistance with Reactance Is Sufficient to Use Eddy Current Technology to Quantify Zirconia Thickness.

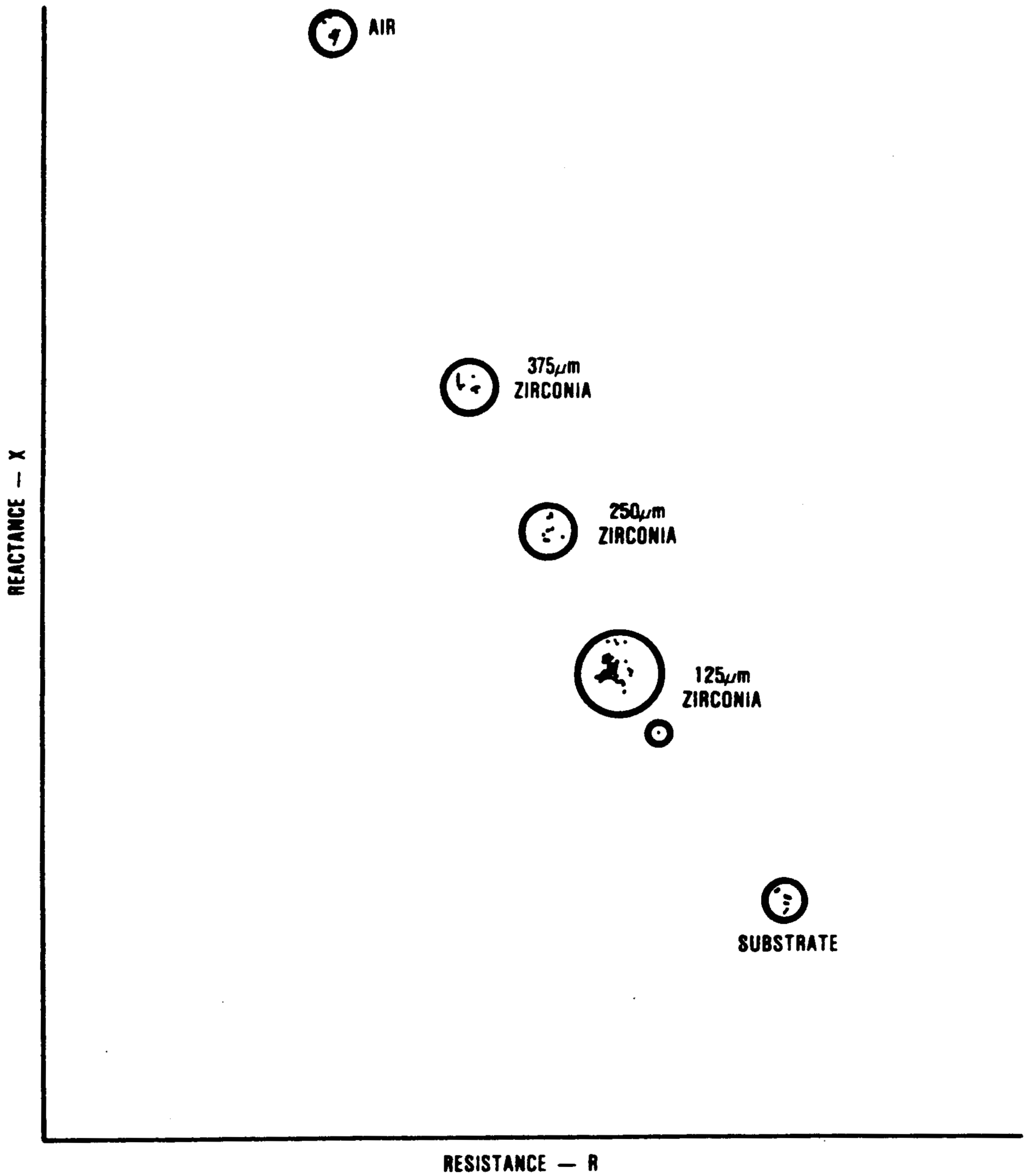

Figure 5-7. Reproducibility of Eddy Current Response Is Good for Chromalloy Thermal Barrier Coating System.

6.0 CONCLUSIONS

The objectives of this program are to develop mission-analysis-capable life models for plasma-sprayed and EB-PVD applied TBC systems. Based on the literature review and initial data obtained in the program, the following preliminary conclusions can be reached:

- Fracture toughness of plasma-sprayed zirconia is dependent on thermal cycling and time at high temperatures. A fracture mechanics model for zirconia spalling as a function of toughness, temperature, and time appears to be feasible. Additional data are being obtained to investigate this approach.

- It appears to be feasible to modify a GTEC-developed oxidation/hot-corrosion life model for metallic coatings to predict TBC lives in terms of engine and mission parameters (e.g., coating temperature, aircraft altitude, turbine pressure). Burner rig data are being obtained to validate this approach.

- Eddy current technology is viable for nondestructively measuring zirconia thickness.

REFERENCES

1. I.E. Sumner and D. Ruckle, "Development of Improved Durability Plasma Sprayed Ceramic Coatings for Gas Turbine Engines," AIAA Paper No. 80-1193, 1980.

2. C.A. Andersson, et al., "Advanced Ceramic Coating Development for Industrial/Utility Gas Turbine Applications," NASA CR-165619, 1982.

3. W.D. Kingery, Introduction to Ceramics, 1960, p. 599.

4. I. Zaplatynsky, "Performance of Laser-Glazed Zirconia Thermal Barrier Coatings in Cyclic Oxidation and Corrosion Burner Rig Tests," Thin Solid Films, 95 (1982), 275-284.

5. E. Demaray, "Thermal Barrier Coatings by Electron Beam Physical Vapor Deposition," DOE Contract DE-AC06-76RL01830, 1982.

6. N.E. Ulion and D.L. Ruckle, "Columnar Grain Ceramic Thermal Barrier Coatings on Polished Substrates," U.S. Patent 4,321,310, 1982.

7. T.E. Strangman, "Columnar Grain Ceramic Thermal Barrier Coatings," U.S. Patent 4,321,331, 1982.

8. D.S. Duval, "Processing Technology for Advanced Metallic and Ceramic Turbine Airfoil Coatings," in Proceedings of the Second Conference on Advanced Materials for Alternative-Fuel-Capable Heat Engines, EPRI RD-2369-SR, Monterey, California, 1981.

9. K.D. Sheffler, R.A. Graziani, and G.C. Sinko, "JT9D Thermal Barrier Coated Vanes," NASA CR-167964, 1982.

10. A.G. Evans, G.C. Crumley, and E. Demaray, "On the Mechanical Behavior of Brittle Coatings and Layers," Oxidation of Metals, 20 (1983), 193-216.

11. T.E. Strangman, "Thermal Barrier Coatings for Turbine Airfoils," Thin Solid Films, 127 (1985), 93-105.

12. R.A. Miller, "An Oxidation Based Model for Thermal Barrier Coating Life," J. American Ceramic Society, 67 (1984), 517-521.

13. R.A. Miller and C.E. Lowell, "Failure Mechanism of Thermal Barrier Coatings Exposed to Elevated Temperatures," Thin Solid Films, 95 (1982), 265-273.

14. T.E. Strangman, "Life Prediction and Development of Coatings for Turbine Airfoils," Workshop or Gas Turbine Materials in a Marine Environment, Bath, England 1984.

15. G. McDonald and R. Hendricks, "Effect of Thermal Cycling on ZrO_2 - Y_2O_3 Thermal Barrier Coatings," NASA TM 81480, 1980.

16. G. McDonald and R. Hendricks, Thin Solid Films, 73 (1980), 491-496.

17. R.A. Miller and C.C. Berndt, "Performance of Thermal Barrier Coatings in High Heat Flux Environments," Thin Solid Films, 119 (1984), 195-202.

18. R.A. Miller, "Analysis of the Response of a Thermal Barrier Coating to Sodium and Vanadium-Doped Combustion Gases," DOE/NASA/2593-79/7, NASA TM-79205, 1979.

GARRETT TURBINE ENGINE COMPANY
A DIVISION OF THE GARRETT CORPORATION
PHOENIX, ARIZONA

DISTRIBUTION LIST

D. L. Alger (301-2)
NASA Lewis Research Center
21000 Brookpark Road
Cleveland, OH 44135

L. F. Aprigliano
D. Taylor Shipyard
R&D Center
Annapolis, MD 21402

M. M. Bailey (77-6)
NASA Lewis Research Center
21000 Brookpark Road
Cleveland, OH 44135

Michael Bak (5-16)
Williams International
P.O. Box 200
Walled Lake, MI 48088

H. Beale
Applied Coatings, Inc.
775 Kaderly Drive
Columbus, OH 43228

Robert Beck
Teledyne - CAE
1330 Laskey Road
Toledo, OH 43612

Biliyar N. Bhat (EH-23)
NASA Marshall Space
Flight Center
Huntsville, AL 35812

Donald H. Boone
University of California
Bldg. 62, Room 351
Berkeley, CA 94720

David Bott
Muscle Shoals Mineral Company
1202 East 2nd Street
Muscle Shoals, AL 35661

R. J. Bratton
Westinghouse Electric R&D
1310 Buelah Road
Pittsburgh, PA 15235

Sherman D. Brown
Chemical Engineering Dept.
University of Illinois
Urbana, IL 61801

Walter Bryzik (RGRD)
U.S. Army Tank-Auto. Command
Diesel Engine Research RMSTA
Warren, MI 48397

R. F. Bunshah
University of California
6532 Boelter Hall
Los Angeles, CA 90024

George C. Chang (MC 219)
Cleveland State University
Cleveland, OH 44115

Jerry Clifford
U.S. Army Applied Tech. Lab.
SAVDL-ATL-ATP
Fort Eustis, VA 23604

Dave Clingman
Detroit Diesel Allison - GMC
Engineering Operations
Indianapolis, IN 46206

DISTRIBUTION LIST (CONTD)

Arthur Cohn
E P R I
3412 Hillview Avenue
Palo Alto, CA 94303

Thomas A. Cruse
Southwest Research Institute
P.O. Box 28510
San Antonio, TX 78284

Keith Duframe
Battelle Labs.
Columbus, OH 43216

Mrityunjoy Dutta
U.S. Army AMSAV-EAS
4300 Goodfellow Blvd.
St. Louis, MO 63120

D. S. Engleby
Naval Air Rework Facility
Mail Drop 9, Code 017
Cherry Point, NC 28533

John Fairbanks (FE-22)
Department of Energy
Office of Fossil Energy
Washington, DC 20545

N. Geyer
AFWAL/MLLM
Wright Patterson AFB
Dayton, OH 45433

J. W. Glatz
NAPTC R&D Division
Naval Air Prop. Test Center
Trenton, NJ 08628

G. W. Goward
Coatings Technology Corp.
2 Commercial Street
Branford, CT 06405

M. A. Greenfield (RM)
NASA Headquarters
600 Independence Avenue
Washington, DC 20546

S. J. Grisaffe (49-1)
NASA Lewis Research Center
21000 Brookpark Road
Cleveland, OH 44135

D. K. Gupta
Pratt & Whitney Aircraft
400 Main Street
E. Hartford, CT 06108

William K. Halman
Temescal
2850 Seventh Street
Berkeley, CA 94710

D. Hanink
Detroit Diesel Allison-GMC
Engineering Operations
Indianapolis, IN 46206

Doug Harris
APS - Materials Inc.
153 Walbrook
Dayton, OH 45405

Harold Herman
Argonne National Lab.
9700 South Cass Avenue
Argonne, IL 60439

DISTRIBUTION LIST (CONTD)

H. Herman (W-8)
Detroit Diesel Allison-GMC
P.O. Box 894
Indianapolis, IN 46206

C. Kortovich
TRW Inc.
23355 Euclid Avenue
Cleveland, OH 44117

M. Herman
Dept. of Materials Science
State Univ. of New York
Stonybrook, NY 11794

Propulsion Laboratory (302-2)
U.S. Army Res. & Tech. Lab.
21000 Brookpark Road
Cleveland, OH 44135

Frank Hermanek
Alloy Metals, Inc.
501 Executive Drive
Troy, MI 48084

Sylvester Lee
AFWAL-MLTM
Wright Patterson AFB
Dayton, OH 45433

R. Hillery (M-85)
General Electric Company
MPTL
Cincinnati, OH 45215

A. V. Levy
Lawrence Berkely Lab.
University of California
Berkeley, CA 94720

J. Stan Hilton
University of Dayton
300 College Park
Dayton, OH 45469

C. H. Liebert (77-2)
NASA Lewis Research Center
21000 Brookpark Road
Cleveland, OH 44135

Richard R. Holmes (EH-43)
Marshall Space
Flight Center
Hunstville, AL 35812

E. L. Long, Jr.
Oak Ridge National Lab.
P.O. Box X, Bldg. 4508
Oak Ridge, TN 37831

Lulu Hsu
Solar Turbines, Inc.
2200 Pacific Highway
San Diego, CA 92138

Frank N. Longo
Metco, Inc.
1101 Prospect Avenue
Westbury, L.I., NY 11590

Larry A. Junod
Allison Gas Turbine Division
P.O. Box 420, Plant 8-T12
Indianapolis, IN 46206

Richard Martin (9W-61)
Boeing Commercial Airplane Co.
P.O. Box 3707
Seattle, WA 98124

DISTRIBUTION LIST (CONTD)

R. A. Miller (105-1)
NASA Lewis Research Center
21000 Brookpark Road
Cleveland, OH 44135

T. E. Mitchell
Case Western Reserve Univ.
10900 Euclid Avenue
Cleveland, OH 44106

S. Naik
AVCO-Lycoming Division
550 South Main Street
Stratford, CT 06497

Dr. J. A. Nesbitt (105-1)
NASA Lewis Research Center
21000 Brookpark Road
Cleveland, OH 44135

J. W. Patten
Cummins Engine Company
Box 3005
Columbus, IN 47202

Ronne D. Proch
Corning Glass Works
31501 Solon Road
Solon, OH 44139

R. J. Quentmeyer (500-220)
NASA Lewis Research Center
21000 Brookpark Road
Cleveland, OH 44135

Gopal Revanton
Deer & Company
3300 River Drive
Moline, IN 61265

David Rigney (D-83)
General Electric Company
Cincinnati, OH 45215

Joseph Scricca
AVCO-Lycoming Division
550 South Main Street
Stratford, CT 06497

Keith Sheffler
Pratt & Whitney Aircraft
400 Main Street
Hartford, CT 06109

T. P. Shyu
Caterpiller Tractor Company
100 N.E. Adams
Peoria, IL 61629

R. W. Soderquist (165-03)
Pratt & Whitney Aircraft
400 Main Street
E. Hartford, CT 06108

D. E. Sokolowski (49-7)
NASA Lewis Research Center
21000 Brookpark Road
Cleveland, OH 44135

C. A. Stearns (106-1)
NASA Lewis Research Center
21000 Brookpark Road
Cleveland, OH 44135

S. Stecura (105-1)
NASA Lewis Research Center
21000 Brookpark Road
Cleveland, OH 44135

DISTRIBUTION LIST (CONTD)

T. E. Strangman
Garrett Turbine Engine Co.
111 South 24th Street
Phoenix, AZ 85034

T. N. Strom (23-2)
NASA Lewis Research Center
21000 Brookpark Road
Cleveland, OH 44135

T. A. Taylor
Linde Division
Union Carbide Corporation
Indianapolis, IN 46224

Robert P. Tolokan
Brunswick Corporation
2000 Brunswick Lane
DeLand, FL 32724

F. C. Toriz
Rolls Royce, Inc.
1985 Phoenix Blvd.
Atlanta, GA 30349

Donald Whicker
GM Research Laboratory
GM Technical Center
Warren, MI 48090

Volker Wilms
Chromalloy R&T
Chromalloy Amer. Corp.
Orangeburg, NY 10962

I. Zaplatynsky (105-1)
NASA Lewis Research Center
21000 Brookpark Road
Cleveland, OH 44135